Check for updates

NIST Technical Note
NIST TN 2305

Performance of New Smoke Alarms and Aerosol Measurements for a Range of Nuisance Cooking Sources in a Mock Kitchen

Amy E. Mensch
Emma M. Veley
Thomas G. Cleary

This publication is available free of charge from:
https://doi.org/10.6028/NIST.TN.2305

NATIONAL INSTITUTE OF STANDARDS AND TECHNOLOGY
U.S. DEPARTMENT OF COMMERCE

NIST Technical Note
NIST TN 2305

Performance of New Smoke Alarms and Aerosol Measurements for a Range of Nuisance Cooking Sources in a Mock Kitchen

Amy E. Mensch
Emma M. Veley
Thomas G. Cleary
Fire Research Division
Engineering Laboratory

This publication is available free of charge from:
https://doi.org/10.6028/NIST.TN.2305

September 2024

U.S. Department of Commerce
Gina M. Raimondo, Secretary

National Institute of Standards and Technology
Laurie E. Locascio, NIST Director and Under Secretary of Commerce for Standards and Technology

Certain equipment, instruments, software, or materials, commercial or non-commercial, are identified in this paper in order to specify the experimental procedure adequately. Such identification does not imply recommendation or endorsement of any product or service by NIST, nor does it imply that the materials or equipment identified are necessarily the best available for the purpose.

NIST Technical Series Policies
Copyright, Use, and Licensing Statements
NIST Technical Series Publication Identifier Syntax

Publication History
Approved by the NIST Editorial Review Board on 2024-09-16

How to cite this NIST Technical Series Publication:
Mensch AM, Veley EM, Cleary TG (2024) Performance of New Smoke Alarms and Aerosol Measurements for a Range of Nuisance Cooking Sources in a Mock Kitchen. (National Institute of Standards and Technology, Gaithersburg, MD), NIST TN 2305. https://doi.org/10.6028/NIST.TN.2305

Author ORCID iDs
Amy E. Mensch: 0000-0002-7202-8518
Emma M. Veley: 0000-0001-7551-2666
Thomas G. Cleary: 0000-0001-8785-2035

Contact Information
amy.mensch@nist.gov

Abstract

New smoke alarms that have passed the broiling hamburger nuisance test introduced in 2015 to ANSI/UL 217 Standard for Safety Smoke Alarms have reached the market. This cooking scenario was selected to be representative of cooking nuisance sources generally. The current study compares the nuisance alarm resistance between new smoke alarms and legacy alarm designs to a variety of cooking scenarios. A series of cooking experiments were conducted with an electric-coil cooktop and oven surrounded by mock cabinets and the smoke alarms mounted on ceiling panels in the mock-kitchen. A variety of smoke alarm types and models were tested, including four smoke alarm models that have passed the current 9th Edition of ANSI/UL 217-2020 and six legacy models, either ionization, photoelectric, or dual-type, certified to the previous Edition. Also during the tests, the aerosols produced from the cooking were characterized using an electrical low pressure cascade impactor to quantify the aerosol concentrations and diameters generated by the nuisance sources during the experiment and at the time of alarm. The alarm activation results showed that the new alarms as a group were not clearly superior in nuisance alarm resistance to the selected cooking scenarios compared to the legacy designs. While the broiling hamburger nuisance test added to ANSI/UL 217 may not be sufficient to prevent nuisance alarms across all cooking scenarios, it does provide a performance baseline to ensure newer alarms that need to meet the more stringent flaming and smoldering fire tests are not overly sensitive to nuisance sources.

Keywords

Cooking aerosols; nuisance alarms; smoke alarms; ANSI/UL 217; particle measurements.

Table of Contents

1. Introduction 1
2. Experimental Methods 1
3. Results 12
3.1. Smoke Alarm Performance 12
3.1.1. Overall Performance by Alarm Model 13
3.1.2. Performance by Cooking Scenario 18
3.2. Aerosol Results 39
4. Conclusion 63
References 65

List of Tables

Table 1. Smoke Alarm Model Information 5
Table 2. Overall Fraction of Cooking Tests Where a Smoke Alarm Signal Was Produced Within the Duration of the Test Plus 120 s. 17
Table 3. Fraction of Cooking Tests Where a Smoke Alarm Signal Was Produced Within the Duration of the Test Plus 120 s, by Smoke Alarm Type, for Each Cooking Scenario and Overall. 19

List of Figures

Fig. 1. Front view of the mock kitchen experimental setup (not to scale). 2
Fig. 2. Top view of the mock kitchen experimental setup. 3
Fig. 3. The velocity near the smoke alarms with the range hood on with error bars showing the measurement standard deviation, $\pm$ 0.1 m/s. 4
Fig. 4. Photos showing the broiling hamburgers scenario (a) in oven prior to heating and (b) after 1200 s of broiling. 7
Fig. 5. Photos showing the frozen pizza scenario (a) in oven prior to heating and (b) after 840 s of broiling. 7
Fig. 6. Photos showing the two toast scenarios (a) regular toast after 180 s of toasting and (b) dark toast after 240 s of toasting. 8
Fig. 7. Photos showing toaster pastries scenario (a) in toaster prior to heating, (b) front side after heating, and (c) back side after heating. 8
Fig. 8. Photos showing the progression of frying bacon, (a) before cooking, (b) at 120 s of cooking, (c) at 330 s of cooking (after flipping), and (d) at the end of cooking (515 s). 9
Fig. 9. Photos showing the frying hamburger scenario (a) after 40 s of cooking the hamburger and (b) at the end, after 510 s cooking the hamburger. 10

Fig. 10. Photos showing the progression of the frozen potato fries scenario, (a) after 20 s of cooking, (b) after 350 s of cooking (after stirring once), (c) after 640 s of cooking (after stirring twice), and (d) at the end of cooking (900 s). 11
Fig. 11. Photos showing the stir-fried vegetables scenario (a) after 30 s of cooking and (b) at the end, after 720 s of cooking. 12
Fig. 12. Photos showing the grilled cheese sandwich scenario (a) before cooking and (b) at the end, after 315 s of cooking. 12
Fig. 13. Overall fraction of cooking tests where a smoke alarm signal was produced for the new smoke alarms as a function of the relative cooking time, with the range hood off. 13
Fig. 14. Overall fraction of cooking tests where a smoke alarm signal was produced for the new smoke alarms as a function of the relative cooking time, with the range hood on. 14
Fig. 15. Overall fraction of cooking tests where a smoke alarm signal was produced for the legacy smoke alarms as a function of the relative cooking time, with the range hood off. 15
Fig. 16. Overall fraction of cooking tests where a smoke alarm signal was produced for the legacy smoke alarms as a function of the relative cooking time, with the range hood on. 16
Fig. 17. Overall fraction of cooking tests where a smoke alarm signal was produced for the reference smoke alarms as a function of the relative cooking time. . 17
Fig. 18. Fraction of broiling hamburger tests where a smoke alarm signal was produced for the reference smoke alarms as a function of the relative cooking time. 20
Fig. 19. Fraction of broiling hamburger tests where a smoke alarm signal was produced for the new smoke alarms as a function of the relative cooking time, with the range hood off. 21
Fig. 20. Fraction of broiling hamburger tests where a smoke alarm signal was produced for the new smoke alarms as a function of the relative cooking time, with the range hood on. 22
Fig. 21. Fraction of broiling hamburger tests where a smoke alarm signal was produced for the legacy smoke alarms as a function of the relative cooking time, with the range hood off. 23
Fig. 22. Fraction of broiling hamburger tests where a smoke alarm signal was produced for the legacy smoke alarms as a function of the relative cooking time, with the range hood on. 24
Fig. 23. Fraction of broiling hamburger tests where a smoke alarm signal was produced for each smoke alarm type, on average, as a function of the relative cooking time, with the range hood off. Shaded region shows the standard deviation in performance for the new alarms. 25
Fig. 24. Fraction of broiling hamburger tests where a smoke alarm signal was produced for each smoke alarm type, on average, as a function of the relative cooking time, with the range hood on. Shaded region shows the standard deviation in performance for the new alarms. 26

Fig. 25. Fraction of frying hamburger tests where a smoke alarm signal was produced for the reference smoke alarms as a function of the relative cooking time. . 27
Fig. 26. Fraction of frying hamburger tests where a smoke alarm signal was produced for the new smoke alarms as a function of the relative cooking time, with the range hood off and on. 28
Fig. 27. Fraction of frying hamburger tests where a smoke alarm signal was produced for each smoke alarm type, on average, as a function of the relative cooking time, with the range hood off. Shaded region shows the standard deviation in performance for the new alarms. 29
Fig. 28. Fraction of frying hamburger tests where a smoke alarm signal was produced for each smoke alarm type, on average, as a function of the relative cooking time, with the range hood on. Shaded region shows the standard deviation in performance for the new alarms. 30
Fig. 29. Fraction of frying bacon tests where a smoke alarm signal was produced for the reference smoke alarms as a function of the relative cooking time. . . . 31
Fig. 30. Fraction of frying bacon tests where a smoke alarm signal was produced for the new smoke alarms as a function of the relative cooking time, with the range hood off. 32
Fig. 31. Fraction of frying bacon tests where a smoke alarm signal was produced for the new smoke alarms as a function of the relative cooking time, with the range hood on. 33
Fig. 32. Fraction of frying bacon tests where a smoke alarm signal was produced for each smoke alarm type, on average, as a function of the relative cooking time, with the range hood off. Shaded region shows the standard deviation in performance for the new alarms. 34
Fig. 33. Fraction of frying bacon tests where a smoke alarm signal was produced for each smoke alarm type, on average, as a function of the relative cooking time, with the range hood on. Shaded region shows the standard deviation in performance for the new alarms. 35
Fig. 34. Fraction of dark toast tests where a smoke alarm signal was produced for the reference smoke alarms as a function of the relative cooking time. 36
Fig. 35. Fraction of dark toast tests where a smoke alarm signal was produced for the new smoke alarms as a function of the relative cooking time, with the range hood off and on. 37
Fig. 36. Fraction of dark toast tests where a smoke alarm signal was produced for each smoke alarm type, on average, as a function of the relative cooking time, with the range hood off. 38
Fig. 37. Fraction of dark toast tests where a smoke alarm signal was produced for each smoke alarm type, on average, as a function of the relative cooking time, with the range hood on. 39
Fig. 38. The relative humidity and temperature at the ceiling for a typical broiling hamburgers test over the cooking time. 40
Fig. 39. The mass concentration and the mass mean diameter over the cooking time of a typical broiling hamburgers test. Symbols indicate when alarm activated and the mass concentration at activation. 41

Fig. 40. The number concentration and the diameter concentration over the cooking time of a typical broiling hamburgers test. Symbols indicate when alarm activated and the number concentration at activation. 41
Fig. 41. Mass concentration at time of alarm (closed symbols) or at maximum mass concentration if no alarm (open symbols) for the N1, N2, N3, and N4 alarms with the hood off (left) and the hood on (right) for the broiling hamburgers tests. 42
Fig. 42. Beam obscuration at time of alarm (closed symbols) or at maximum obscuration if no alarm (open symbols) for the N1, N2, N3, and N4 alarms with the hood off (left) and the hood on (right) for all broiling hamburgers tests. . . . 43
Fig. 43. The mass concentration and the mass mean diameter over the cooking time of a typical frozen pizza test. Symbols indicate when alarm activated and the mass concentration at activation. 44
Fig. 44. The number concentration and the diameter concentration over the cooking time of a typical frozen pizza test. Symbols indicate when alarm activated and the number concentration at activation. 44
Fig. 45. Mass concentration at time of alarm (closed symbols) or at maximum mass concentration if no alarm (open symbols) for the N1, N2, N3, and N4 alarms with the hood off (left) and the hood on (right) for all frozen pizza tests. . . . 45
Fig. 46. The mass concentration and the mass mean diameter over the cooking time of one of a typical regular toast test. Symbols indicate when alarm activated and the mass concentration at activation. 46
Fig. 47. The number concentration and the diameter concentration over the cooking time of one of a typical regular toast test. Symbols indicate when alarm activated and the number concentration at activation. 46
Fig. 48. Mass concentration at time of alarm (closed symbols) or at maximum mass concentration if no alarm (open symbols) for the N1, N2, N3, and N4 alarms with the hood off (left) and the hood on (right) for all regular toast tests. . . 47
Fig. 49. The mass concentration and the mass mean diameter over the cooking time of one of the dark toast scenarios. Symbols indicate when alarm activated and the mass concentration at activation. 48
Fig. 50. The number concentration and the diameter concentration over the cooking time of one of the dark toast scenarios. Symbols indicate when alarm activated and the number concentration at activation. 48
Fig. 51. Mass concentration at time of alarm (closed symbols) or at maximum mass concentration if no alarm (open symbols) for the N1, N2, N3, and N4 alarms with the hood off (left) and the hood on (right) for all dark toast tests. 49
Fig. 52. The mass concentration and the mass mean diameter over the cooking time of one of the toaster pastries tests. No smoke alarms activated during this particular test. 50
Fig. 53. The number concentration and the diameter concentration over the cooking time of one of the toaster pastries tests. No smoke alarms activated during this particular test. 50

Fig. 54. Mass concentration at time of alarm (closed symbols) or at maximum mass concentration if no alarm (open symbols) for the N1, N2, N3, and N4 alarms with the hood off (left) and the hood on (right) for all toaster pastries tests. 51
Fig. 55. The mass concentration and the mass mean diameter over the cooking time of a typical frying bacon test. Symbols indicate when alarm activated and the mass concentration at activation. 52
Fig. 56. The number concentration and the diameter concentration over the cooking time of a typical frying bacon test. Symbols indicate when alarm activated and the number concentration at activation. 52
Fig. 57. Mass concentration at time of alarm (closed symbols) or at maximum mass concentration if no alarm (open symbols) for the N1, N2, N3, and N4 alarms with the hood off (left) and the hood on (right) for all frying bacon tests. . . 53
Fig. 58. Beam obscuration at time of alarm (closed symbols) or at maximum obscuration if no alarm (open symbols) for the N1, N2, N3, and N4 alarms with the hood off (left) and the hood on (right) for all frying bacon tests. 54
Fig. 59. The mass concentration and the mass mean diameter over the cooking time of one of the frying hamburger scenarios. Symbols indicate when alarm activated and the mass concentration at activation. 55
Fig. 60. The number concentration and the diameter concentration over the cooking time of one of the frying hamburger scenarios. Symbols indicate when alarm activated and the number concentration at activation. 55
Fig. 61. Mass concentration at time of alarm (closed symbols) or at maximum mass concentration if no alarm (open symbols) for the N1, N2, N3, and N4 alarms with the hood off (left) and the hood on (right) for all frying hamburger tests. 56
Fig. 62. Beam obscuration at time of alarm (closed symbols) or at maximum obscuration if no alarm (open symbols) for the N1, N2, N3, and N4 alarms with the hood off (left) and the hood on (right) for all frying hamburger tests. 57
Fig. 63. The mass concentration and the mass mean diameter over the cooking time of one of the stir-fried vegetables scenarios. Symbols indicate when alarm activated and the mass concentration at activation. 58
Fig. 64. The number concentration and the diameter concentration over the cooking time of one of the stir-fried vegetables scenarios. Symbols indicate when alarm activated and the number concentration at activation. 58
Fig. 65. Mass concentration at time of alarm (closed symbols) or at maximum mass concentration if no alarm (open symbols) for the N1, N2, N3, and N4 alarms with the hood off (left) and the hood on (right) for all stir-fried vegetables tests. 59
Fig. 66. The mass concentration and the mass mean diameter over the cooking time of one of the frozen potato fries tests. Symbols indicate when alarm activated and the mass concentration at activation. 60
Fig. 67. The number concentration and the diameter concentration over the cooking time of one of the frozen potato fries tests. Symbols indicate when alarm activated and the number concentration at activation. 60

Fig. 68. Mass concentration at time of alarm (closed symbols) or at maximum mass concentration if no alarm (open symbols) for the N1, N2, N3, and N4 alarms with the hood off (left) and the hood on (right) for all frozen potato fries tests. 61
Fig. 69. The mass concentration and the mass mean diameter over the cooking time of one of the grilled cheese scenarios. Symbols indicate when alarm activated and the mass concentration at activation. 62
Fig. 70. The number concentration and the diameter concentration over the cooking time of one of the grilled cheese scenarios. Symbols indicate when alarm activated and the number concentration at activation. 62
Fig. 71. Mass concentration at time of alarm (closed symbols) or at maximum mass concentration if no alarm (open symbols) for the N1, N2, N3, and N4 alarms with the hood off (left) and the hood on (right) for all grilled cheese tests. . 63

Author Contributions

Amy E. Mensch: Writing-Original draft preparation, Methodology, Data analysis. **Emma M. Veley**: Data analysis, Visualization, Writing-Original draft preparation. **Thomas G. Cleary**: Conceptualization, Methodology, Writing-Reviewing and Editing.

1. Introduction

New smoke alarms that have passed the new flaming and smoldering fire tests and cooking nuisance test in the ANSI/UL 217 Standard for Smoke Alarms [1] have begun to reach the market. Two new fire tests and a nuisance test had been added to ANSI/UL 217 in 2015 to address concerns about smoke alarm response. Flaming and smoldering polyurethane foam tests were added to represent a common fuel component in residential fires. An additional nuisance test was included to ensure new alarms would not activate for a representative cooking scenario, for which broiling hamburgers was chosen. From June 2024 on, all smoke alarms must pass the two new fire tests and a broiling hamburger nuisance test to be certified to the current Edition of ANSI/UL 217-2020 [1]. The performance of smoke alarms was evaluated in a 2016 report by Cleary [2], which included a wide range of cooking scenarios, consisting of broiling hamburgers, frying hamburgers, stir-frying vegetables, and toasting bread. The study evaluated the performance of smoke alarms that were on the market at the time and had been tested to the previous edition of ANSI/UL 217 (before 2015), hereafter referred to as ”legacy” alarms. The study concluded that most likely no legacy smoke alarm models would meet all the new performance tests [2]. Cleary also reported significant variations across the different nuisance cooking sources in measurements of aerosol production rates, beam obscuration, and ionization response [2]. The nuisance sources produced particles with mass mean diameters ranging from 0.41 µm (broiling hamburgers) to 0.77 µm (dark toast) [3]. Although the broiling hamburger nuisance test seemed to be one of the most conservative scenarios, it was an open question whether this single nuisance cooking test was sufficient to prevent nuisance alarms for a wide range of cooking activities. The current study compares the nuisance resistance between new and legacy smoke alarms for a variety of nuisance cooking scenarios and present additional data gathered on aerosol concentration and size distributions measured when nuisance alarms occur for both legacy and new alarms.

2. Experimental Methods

A series of experiments were conducted in a mock-kitchen depicted in Figs. 1 and 2, with an electric-coil cooktop and electric oven surrounded by mock cabinets and countertop constructed from gypsum board. A range hood shown in Fig. 1 was used in half of the tests on the highest fan setting. The range hood pulled effluent through a grease filter and directed it back toward the center of the room through a vent. The flow velocity measured by an anemometer 5 cm below the grease filter was 1.6 m/s ± 0.7 m/s for the highest range hood fan setting. The cooktop burners were designed with a temperature sensor to meet the new Coil Surface Unit Cooking Oil Ignition Test in UL 858 Standard for Household Electric Ranges [4]. This safety system automatically cycles the burner off and on to limit the burner temperature. In some cooking scenarios, the burner automatically cycled off before the food was cooked to well-done. Therefore, an additional standalone electric-coil burner that would not cycle off and on, with a heat output of 1.1 kW, was placed in the

center of the cooktop (see Fig. 2) and used for most of the cooktop scenarios. The front left 0.86 kW burner on the cooktop was used for frying bacon, since this scenario generally produced enough aerosol to activate some smoke alarms before the automatic burner shut-off. A toaster was placed on the countertop, 8 cm to the right of the cooktop and 8 cm from the front edge of the countertop for toasting bread and toaster pastries. After each experiment, a large fan was turned on that ventilated the room through a ventilation opening on the side wall of the room near smoke alarm position 1, shown in Fig. 2. The fan was off during experiments.

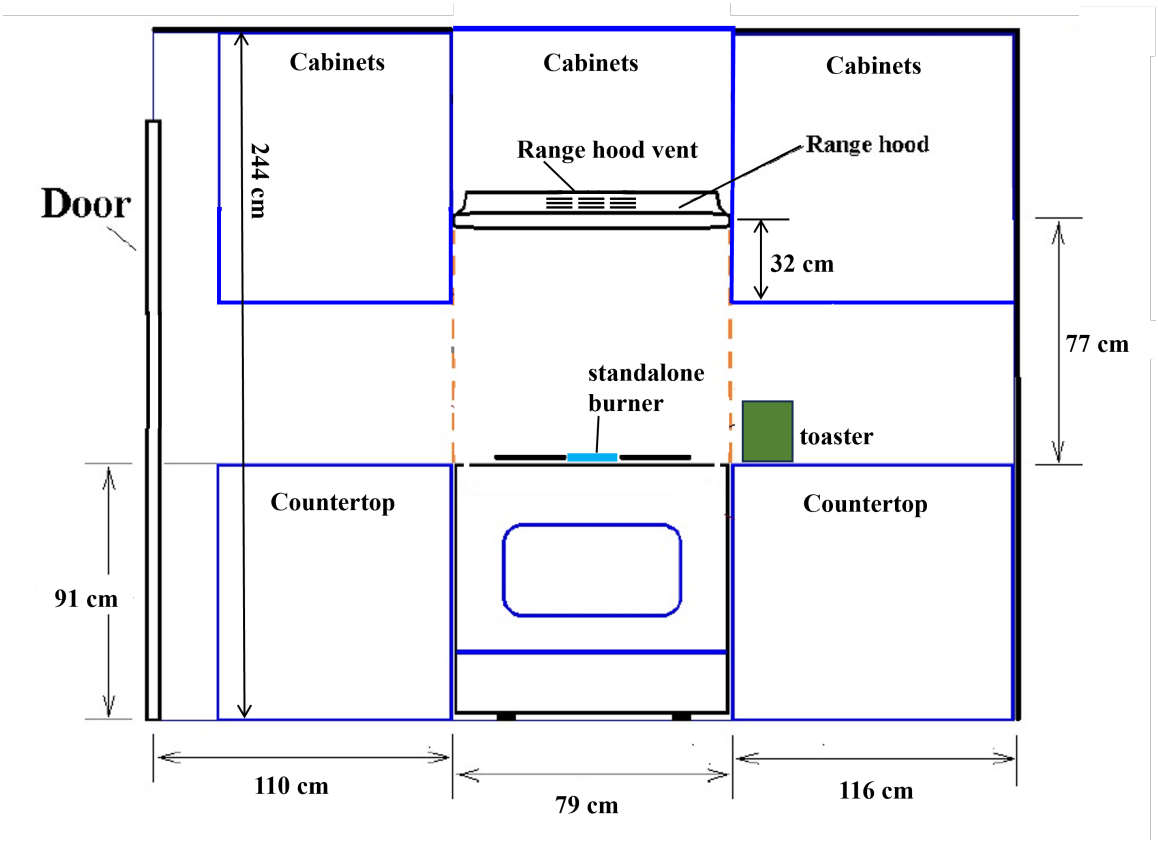

Fig. 1. Front view of the mock kitchen experimental setup (not to scale).

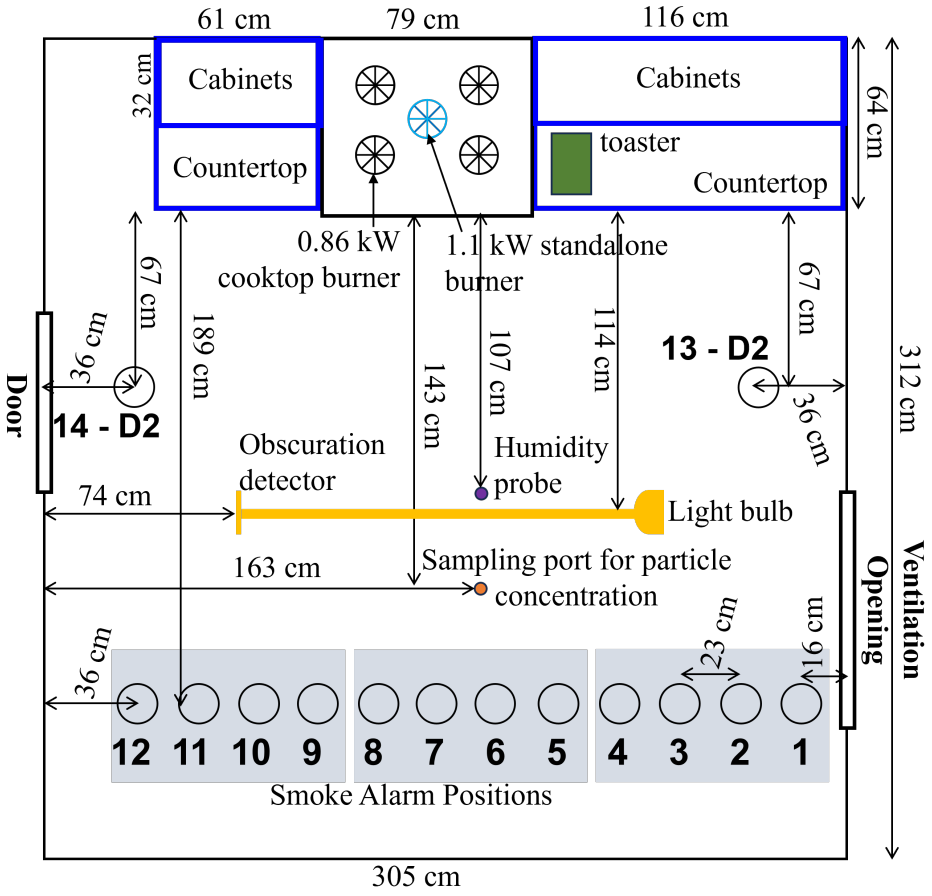

Fig. 2. Top view of the mock kitchen experimental setup.

The background air velocity in front of each smoke alarm position was measured using a hotwire anemometer with the range hood both on and off prior to any cooking activity. The probe was positioned to measure the velocity entering the smoke alarm and parallel to the ceiling, and the probe was located 2.5 cm below the ceiling and 2.5 cm in front of each smoke alarm. With the range hood off, the air velocity near the smoke alarms was low, with an average value of 0.1 m/s $\pm$ 0.1 m/s. There was greater variation in the air velocity between the different smoke alarm positions when the range hood was on. Figure 3 shows the measured velocity by smoke alarm position. The velocity was greatest in the center of the room reaching 1 m/s and lowest near the side walls where the velocity was closer to that when the vent hood was off.

Samples of the aerosols produced from the cooking activities were collected from a sampling port located 143 cm from the front of the cooktop and in front of the row of smoke alarms; the location of the sampling port is displayed in Fig. 2. The particle size distribution and concentration of the aerosol sample were measured using an electrical low-pressure impactor (ELPI). The ELPI charged the particles prior to passing them through 14 impactor

stages [5]. The charge at each of the 14 stages was measured to obtain the number concentration and the aerodynamic diameter of particles across a total range of 6 nm to 10 µm [5] at a rate of 1 Hz. The diameter concentration and mass concentration were also computed. The density of the particles was assumed to be 1 g/cm^3 for all cooking activities. The concentration uncertainty ranged from $\pm$ 20 % for the small diameter particles to $\pm$ 12 % for the large diameter particles [6].

Other measurements within the mock kitchen include temperature, humidity, and smoke obscuration, which can be related to the sensitivity of photoelectric sensors used in some smoke alarms. A humidity probe was located 13 cm below the ceiling, 107 cm from the front of the cooktop and in line with the sampling port to monitor the temperature and humidity throughout the tests (see Fig. 2). Smoke obscuration was measured with a detector mounted 152.4 cm from a light bulb, both 10 cm from the ceiling, and 114 cm from the front of the cooktop. This is the same type of light beam obscuration meter that is part of the ANSI/UL 217 smoke box test for smoke alarm sensitivity to cotton wick smoke [1]. Throughout this report the units of obscuration are reported in English units of %/ft as is industry practice in the United States.

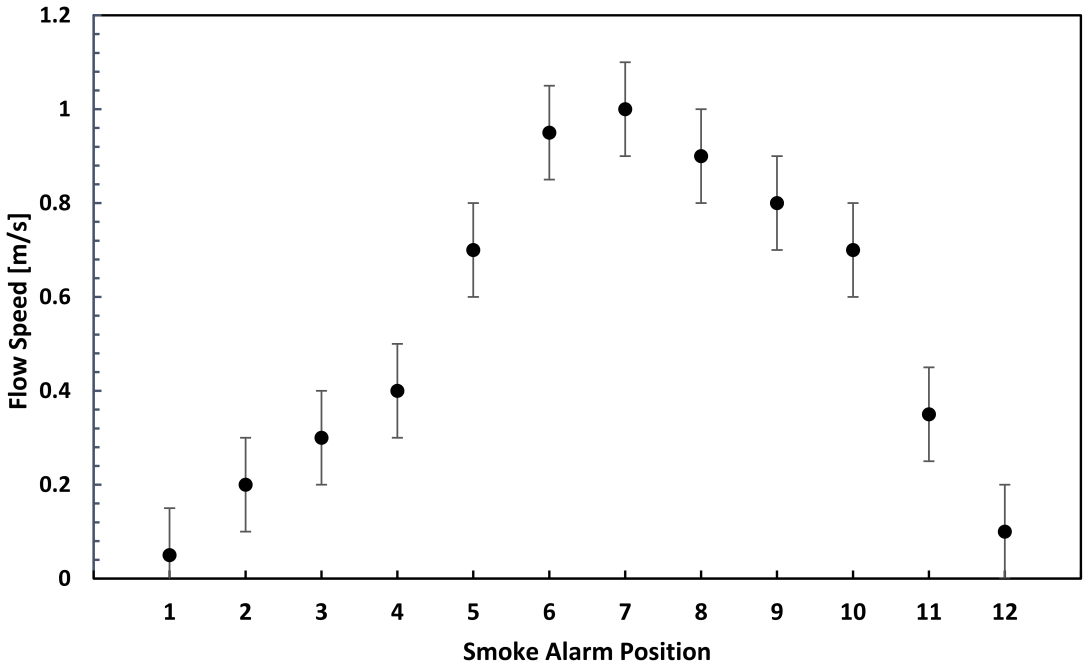

Fig. 3. The velocity near the smoke alarms with the range hood on with error bars showing the measurement standard deviation, $\pm$ 0.1 m/s.

A variety of smoke alarm types and models were tested, including four smoke alarm models that have passed the current 9th Edition of ANSI/UL 217-2020 (N1, N2, N3, N4) and

six legacy alarm models that were produced prior to the requirement to pass the new fire and nuisance tests in ANSI/UL 217-2020. In particular, since the four new alarms are certified to the current ANSI/UL 217-2020 standard, the alarms would have passed the broiling hamburger nuisance test, which does not allow an alarm signal to be produced when the smoke obscuration is at or below 1.5 %/ft [1]. No individual alarms nor manufacturers are identified; NIST does not conduct such product testing. Instead the smoke alarms are assigned ID codes. Two of the new alarms, N1 and N4, are assumed to have ionization sensors in them due to radioactive material markings on the units. The other two new sensors, N2 and N3, did not have radioactive material markings on the units and presumably employ light-scattering sensors. The model ID codes used in this report are given in Table 1 along with the alarm type and power source. The six legacy alarm models included two ionization models (I1, I2), two photoelectric models (P1, P2), and two dual ionization and photoelectric models (D1, D2). Each test had 12 smoke alarms mounted 189 cm from the front of the cooktop across three ceiling panels as shown in Fig. 2. The 12 alarms consisted of one of each smoke alarm model, plus an additional D1 and D2. The three panels, which each had four alarms, were shifted to another panel location in repeat tests to average out location effects. Two additional D2 smoke alarms were mounted closer to the cooking sources, in positions 13 and 14, as a check for test consistency. Two repeat tests were conducted for each configuration, for a total of six tests at each cooking scenario and range hood configuration. The test series was completed both with the range hood off and the range hood exhaust on its highest fan setting. Almost all smoke alarm models were hardwired, and the time when the alarm signal was produced was determined through the electrical interconnect signal. For model N2, where a hardwired version was not available, the alarm time was obtained visually. Data on smoke alarm activation was collected during the cooking scenario and for 120 s after the cooking was complete.

Table 1. Smoke Alarm Model Information

Model ID Code	Alarm Type	Power Source
N1	new, ionization[a]	120 V AC plus battery backup
N2	new, photoelectric[b]	battery
N3	new, photoelectric[b]	120 V AC plus battery backup
N4	new, ionization[a]	120 V AC plus battery backup
I1	legacy, ionization	120 V AC plus battery backup
I2	legacy, ionization	120 V AC plus battery backup
P1	legacy, photoelectric	120 V AC plus battery backup
P2	legacy, photoelectric	120 V AC plus battery backup
D1	legacy, dual ionization and photoelectric	120 V AC plus battery backup
D2	legacy, dual ionization and photoelectric	120 V AC plus battery backup

[a]Presumed based on radioactive material marking on the unit.

[b]Presumed because no radioactive material markings found on the unit.

The nuisance cooking sources tested in this study included broiling hamburgers plus a wider range of foods, including broiling frozen pizza, toasting bread and toaster pastries,

and frying various foods (bacon, a hamburger, frozen potato fries, stir-fried vegetables, and a grilled cheese sandwich) in a 20 cm (8 in) diameter pan or pot on an electric-coil burner. Overall, the test series consisted of 10 cooking scenarios, listed below, that were representative of normal cooking. The cooked foods could be considered well-done, but without excessive charring, and no ignition of the foods. The first scenario was broiling hamburgers, similar to the nuisance test in ANSI/UL 217 9th Edition. The toasting bread scenarios were conducted using a toaster hardwired to apply heat whenever connected to power. The frying bacon scenario used the 0.86 kW cooktop burner, but all other frying scenarios used the 1.1 kW standalone burner.

- **Broiling Hamburgers:** Two frozen 80 % lean hamburgers (approximately 114 g each) were placed in the oven on a broiler pan on the shelf 14 cm below the upper heating elements, and the oven door remained ajar about 8 cm. The oven was set to high broil mode for 1200 s (20 min). See Fig. 4.
- **Frozen Pizza:** One individual-sized (15 cm diameter) frozen pizza was broiled on high for 840 s (14 min). The pizza was placed on a sheet of aluminum foil on the oven shelf 14 cm below the heating elements. See Fig. 5.
- **Regular Toast:** Two slices of white bread (approximately 29 g each) were toasted on the highest setting for 180 s, which was the approximate toasting time before the toaster was hardwired. See Fig. 6a.
- **Dark Toast:** Two slices of white bread (approximately 29 g each) were toasted on the highest setting for 240 s to achieve dark brown, but not black, toast. See Fig. 6b.
- **Toaster Pastries:** Two toaster pastries were placed horizontally in the toaster and toasted on the highest setting for 180 s. See Fig. 7.
- **Frying Bacon:** Two slices of bacon (approximately 61 g total), cut in half for four total pieces, were placed in the stainless steel pan. The bacon was cooked on the highest burner setting on the 0.86 kW cooktop burner for 300 s, flipped, and then cooked until the automatic shut-off (115 s to 215 s more). See Fig. 8.
- **Frying Hamburger:** 30 mL of soybean oil was heated in the stainless steel pan on the highest setting on the standalone burner for 100 s. Then one frozen hamburger (approximately 114 g) was placed on the oil and cooked on high for 180 s, cooked on half-power for 150 s, flipped, and cooked on half-power for 180 s. See Fig. 9.
- **Frozen Potato Fries:** 45 mL of soybean oil was heated on high on the standalone burner for 120 s in a 2.8 L saucepan; then about 167 g of frozen fries were spread in a single layer over the oil. The fries were heated on high for 900 s and flipped every 300 s. See Fig. 10.
- **Stir-Fried Vegetables:** 45 mL of soybean oil was heated on high on the standalone burner for 120 s in the stainless steel pan; then the chopped, raw vegetables (ap-

proximately 67 g onion, 68 g celery, and 36 g carrot) were spread across the oil. The vegetables were heated on high for 720 s and stirred every 60 s. See Fig. 11.

- **Grilled Cheese Sandwich:** The sandwich was prepared with two slices of American cheese inside two slices of white bread (approximately 29 g each). Each slice of bread was coated on the outside with about 7.7 g of vegetable oil spread (about 15.3 g total). The sandwich was heated in the stainless steel pan on high on the standalone burner for 180 s, flipped, heated on high for 100 s, flipped again, and heated on high another 35 s. See Fig. 12.

(a) **(b)**

Fig. 4. Photos showing the broiling hamburgers scenario (a) in oven prior to heating and (b) after 1200 s of broiling.

(a) **(b)**

Fig. 5. Photos showing the frozen pizza scenario (a) in oven prior to heating and (b) after 840 s of broiling.

(a) (b)

Fig. 6. Photos showing the two toast scenarios (a) regular toast after 180 s of toasting and (b) dark toast after 240 s of toasting.

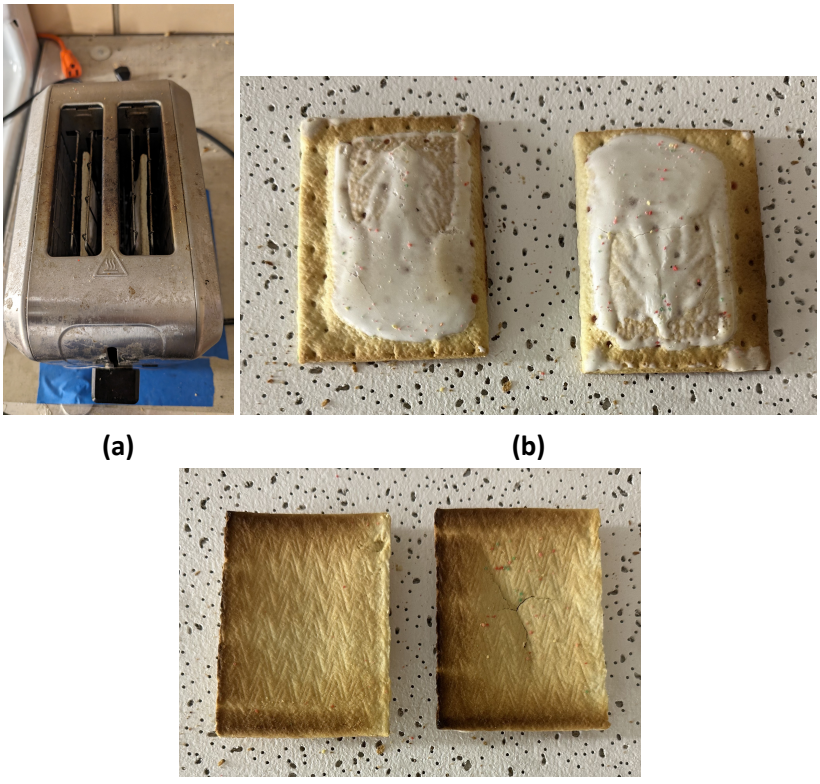

(a) (b)

(c)

Fig. 7. Photos showing toaster pastries scenario (a) in toaster prior to heating, (b) front side after heating, and (c) back side after heating.

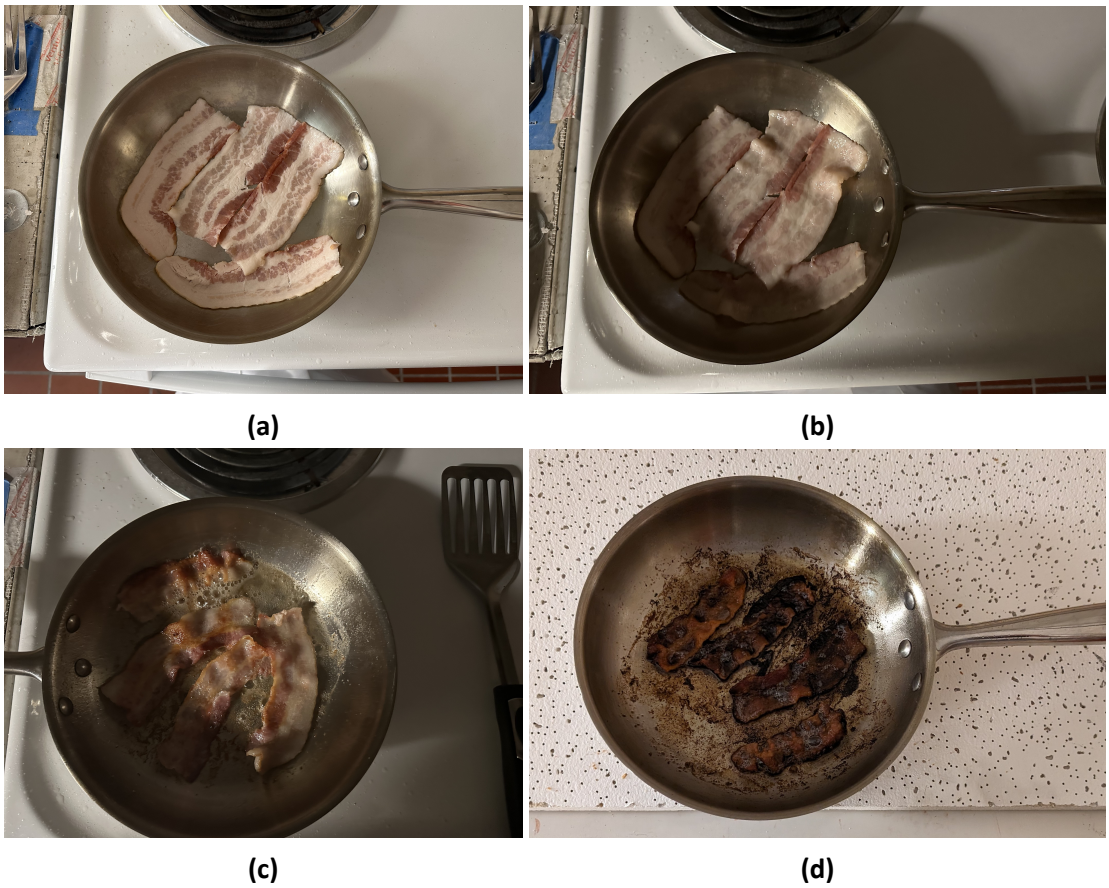

Fig. 8. Photos showing the progression of frying bacon, (a) before cooking, (b) at 120 s of cooking, (c) at 330 s of cooking (after flipping), and (d) at the end of cooking (515 s).

(a) **(b)**

Fig. 9. Photos showing the frying hamburger scenario (a) after 40 s of cooking the hamburger and (b) at the end, after 510 s cooking the hamburger.

Fig. 10. Photos showing the progression of the frozen potato fries scenario, (a) after 20 s of cooking, (b) after 350 s of cooking (after stirring once), (c) after 640 s of cooking (after stirring twice), and (d) at the end of cooking (900 s).

(a) **(b)**

Fig. 11. Photos showing the stir-fried vegetables scenario (a) after 30 s of cooking and (b) at the end, after 720 s of cooking.

(a) **(b)**

Fig. 12. Photos showing the grilled cheese sandwich scenario (a) before cooking and (b) at the end, after 315 s of cooking.

3. Results

3.1. Smoke Alarm Performance

Overall, 120 cooking tests were conducted, 60 with the range hood off and 60 with the range hood on. Smoke alarm performance was evaluated by tracking the fraction of tests where an alarm signal was produced up to a certain percentage of the cooking time. A

value of 1 means the smoke alarm was activated for all tests, and a value of 0 means the smoke alarm was not activated in any tests. Figures in Sections 3.1.1 and 3.1.2 plot the fraction of alarms produced as a function of the relative cooking time, defined as the cooking time over the total cooking time.

3.1.1. Overall Performance by Alarm Model

Figures 13 - 17 plot the fraction of alarms produced with each smoke alarm model shown separately. First are the overall results for the four new alarms with the hood off, Fig. 13, and with the hood on, Fig. 14. The overall results for the six legacy alarms are in Fig. 15 with the hood off and Fig. 16 with the hood on. Finally, Fig. 17 shows the overall results for the two reference alarms that were closer to the cooking sources, in positions 13 and 14. On the far right of each figure is the overall fraction of alarms produced over the entire cooking time plus an additional 120 s for each smoke alarm model, with range hood either off or on. These overall values are also listed in Table 2 for each smoke alarm model to provide a measure of the overall performance for the entire duration of the test plus 120 s. In Figs. 13 - 17 and Table 2 the values reported for D1 and D2 are each an average of two smoke alarms, since there are two of each dual-type model in each test.

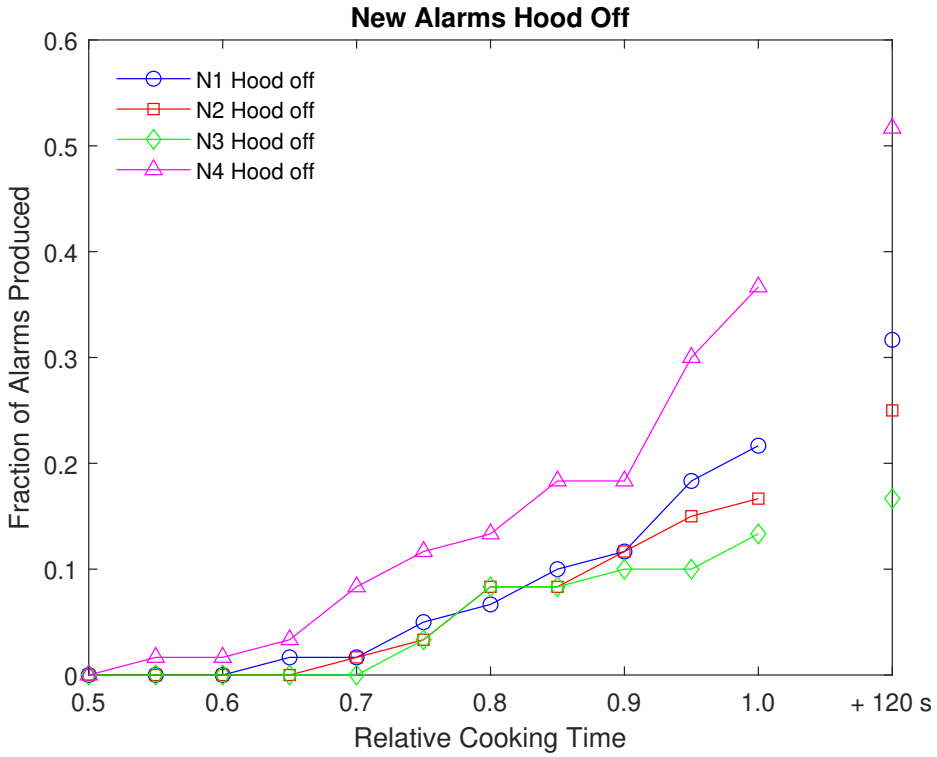

Fig. 13. Overall fraction of cooking tests where a smoke alarm signal was produced for the new smoke alarms as a function of the relative cooking time, with the range hood off.

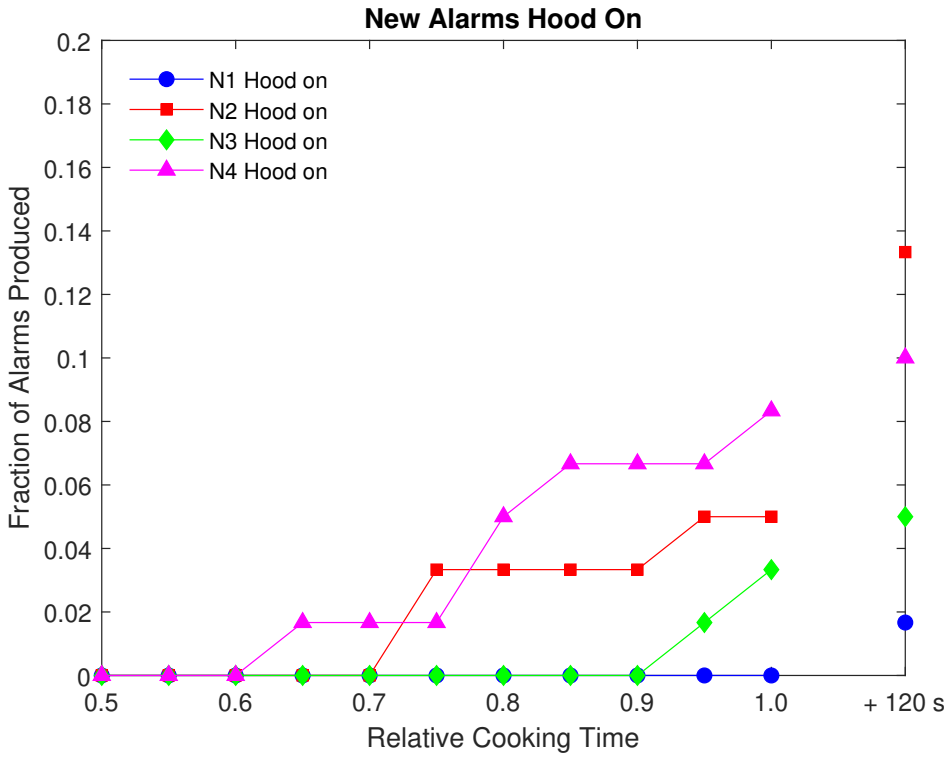

Fig. 14. Overall fraction of cooking tests where a smoke alarm signal was produced for the new smoke alarms as a function of the relative cooking time, with the range hood on.

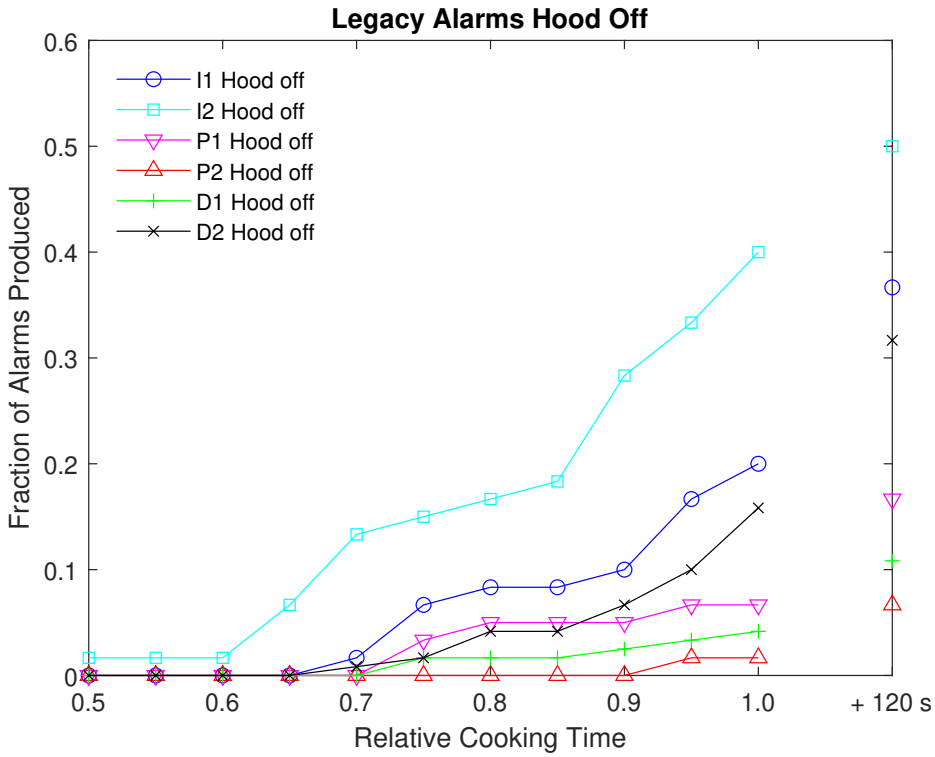

Fig. 15. Overall fraction of cooking tests where a smoke alarm signal was produced for the legacy smoke alarms as a function of the relative cooking time, with the range hood off.

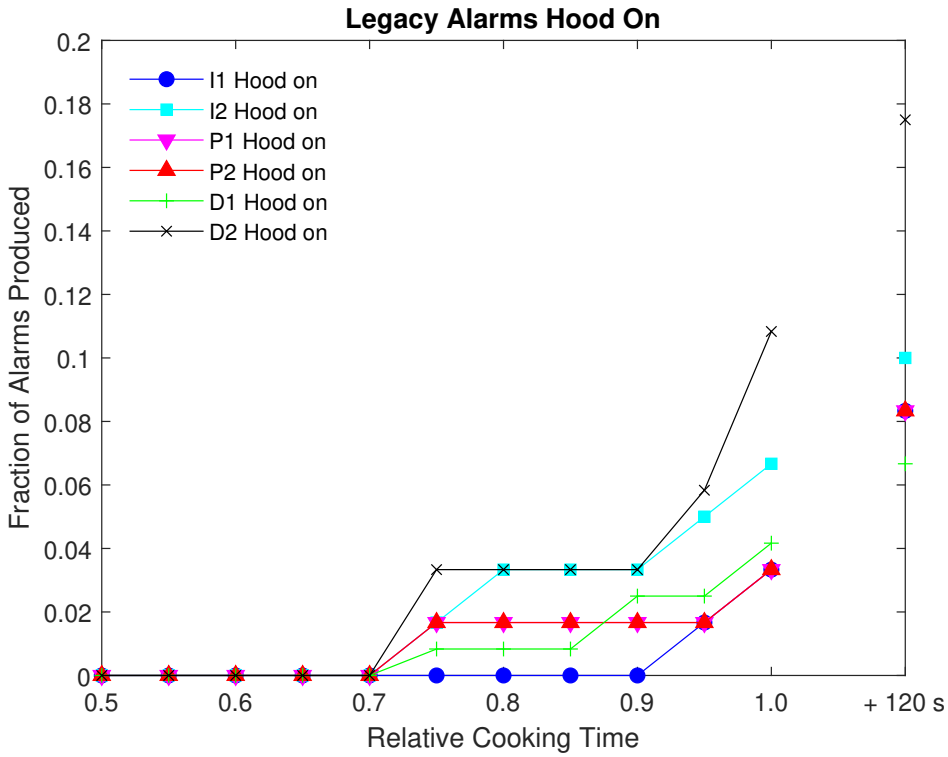

Fig. 16. Overall fraction of cooking tests where a smoke alarm signal was produced for the legacy smoke alarms as a function of the relative cooking time, with the range hood on.

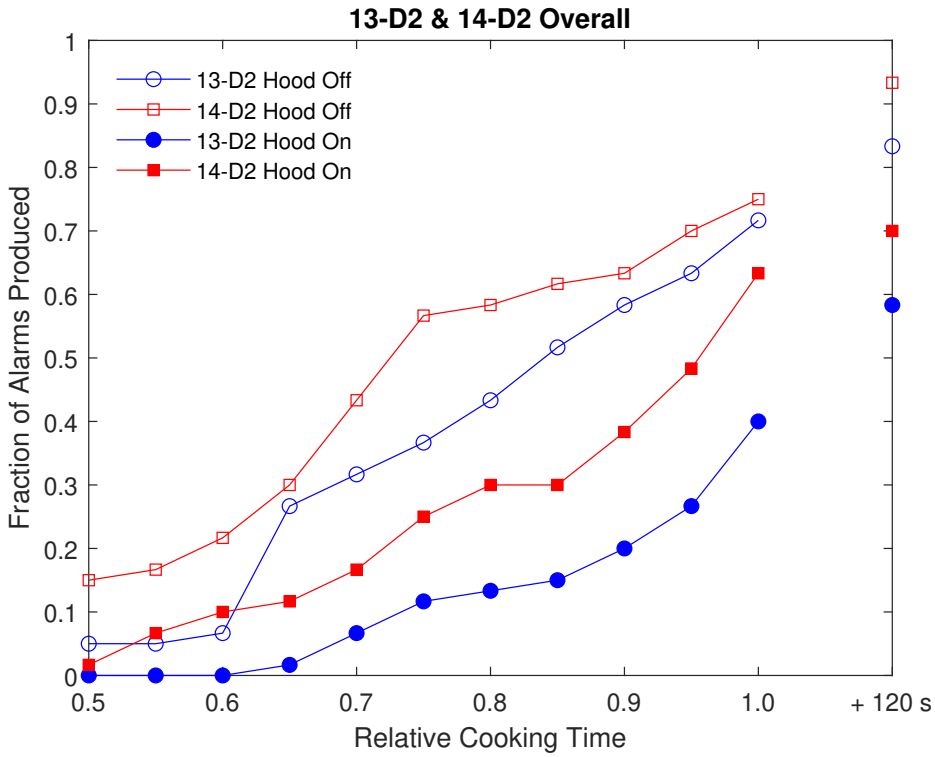

Fig. 17. Overall fraction of cooking tests where a smoke alarm signal was produced for the reference smoke alarms as a function of the relative cooking time.

Table 2. Overall Fraction of Cooking Tests Where a Smoke Alarm Signal Was Produced Within the Duration of the Test Plus 120 s.

Model	Range Hood Off	Range Hood On
N1	0.32	0.02
N2	0.25	0.13
N3	0.17	0.05
N4	0.52	0.10
I1	0.37	0.08
I2	0.50	0.10
P1	0.17	0.08
P2	0.07	0.08
D1 (x2)	0.11	0.07
D2 (x2)	0.32	0.18
13-D2	0.83	0.58
14-D2	0.93	0.70

From Table 2, the legacy photoelectric model, P2, had the lowest fraction of alarm signals with the range hood off. Other alarms that produced an alarm for less than 20 % of the tests

with the hood off were N3, P1, and D1. N2 and N3 did not contain radioactive material and were presumably light-scattering sensor designs. Of the new alarms, N2 and N3 performed best with the range hood off and performed better than the legacy ionization alarms. With the range hood on, performance improved for almost all the models, suggesting that the mixing from the range hood tended to dilute the concentration of cooking aerosols on average. Models that produced alarm signals for less than 10 % of the tests with the range hood on were N1, N3, I1, P1, P2, and D1.

3.1.2. Performance by Cooking Scenario

While Section 3.1.1 reported the overall performance across all cooking scenarios, some scenarios consistently produced alarm signals, while other scenarios generated almost none, as shown in Table 3, which breaks down the final fraction of activations by cooking scenario and smoke alarm type. The alarm activation data throughout the tests are discussed in more detail in this section for the scenarios with the most alarm signals: broiling hamburgers, frying hamburger, frying bacon, and dark toast.

Table 3. Fraction of Cooking Tests Where a Smoke Alarm Signal Was Produced Within the Duration of the Test Plus 120 s, by Smoke Alarm Type, for Each Cooking Scenario and Overall.

Model Type	Range Hood Off	Range Hood On	Range Hood Off	Range Hood On
	Broiling Hamburgers (1200 s cooking time)		Frying Bacon (∼450 s cooking time)	
New	0.46	0.25	0.83	0.25
Ion	0.75	0.50	0.92	0.08
Photo	0.17	0.25	0.75	0.42
Dual	0.50	0.54	0.67	0.33
	Frozen Pizza (840 s cooking time)		Frying Hamburgers (610 s cooking time)	
New	0.08	0.04	0.71	0.08
Ion	0.17	0.08	0.58	0
Photo	0	0	0.25	0.17
Dual	0.08	0	0.25	0.21
	Regular Toast (180 s cooking time)		Frozen Potato Fries (1020 s cooking time)	
New	0.25	0	0.13	0.04
Ion	0.42	0.08	0.42	0
Photo	0	0	0	0
Dual	0.04	0	0	0
	Dark Toast (240 s cooking time)		Stir-Fried Vegetables (840 s cooking time)	
New	0.50	0.11	0.04	0
Ion	1.00	0.21	0	0
Photo	0	0	0	0
Dual	0.58	0.14	0	0
	Toaster Pastries (180 s cooking time)		Grilled Cheese Sandwich (315 s cooking time)	
New	0.13	0	0	0
Ion	0.08	0	0	0
Photo	0	0	0	0
Dual	0	0	0	0
			Overall	
New			0.31	0.08
Ion			0.43	0.09
Photo			0.12	0.08
Dual			0.21	0.12

The broiling hamburgers scenario was similar to the ANSI/UL 217 cooking nuisance test, which all the new alarms have passed, with the most significant difference being this study is conducted in a much smaller room and with the alarms closer to the cooking sources [1].

The results for the broiling hamburger tests are given in Figs. 18 - 22, which plot the fraction of alarms produced for each smoke alarm model as a function of relative cooking time. From the reference alarm results in Fig. 18, it can be seen that both reference alarms were activated in every test, but the alarm in location 14, by the door, tended to activate earlier. The new smoke alarms performed relatively similarly with the range hood off in Fig. 19 and range hood on in Fig. 20. Figure 21 shows the broiling hamburger performance for each legacy alarm with the range hood off. It is observed that the legacy ionization alarms had the highest fraction of alarms produced, followed by the legacy dual-type alarms, and the legacy photoelectric alarms. With the range hood on in Fig. 22, the order of performance is similar, but there are fewer alarms produced. The range hood flow generally decreased the fraction of alarms produced in broiling hamburger tests, but not for all models. Alarm activations actually slightly increased for models P1 and D1 when the range hood was turned on (Fig. 21 and 22). It was not unexpected for the range hood flow to have less overall effect for this oven scenario cooktop scenarios because the effluent coming from the oven is farther away from the range hood opening.

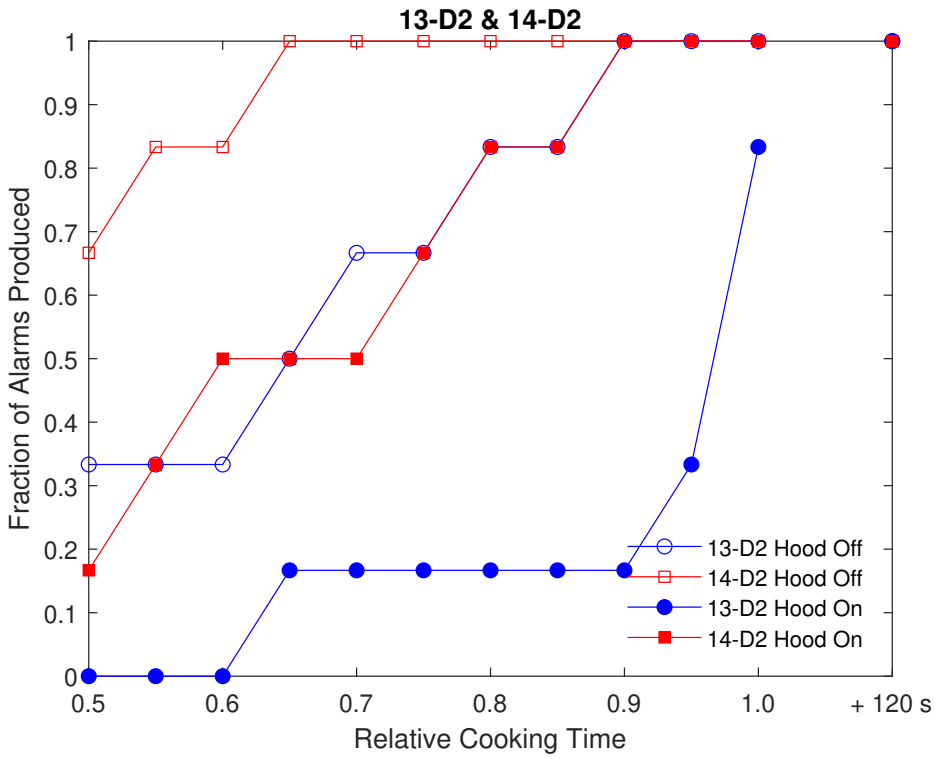

Fig. 18. Fraction of broiling hamburger tests where a smoke alarm signal was produced for the reference smoke alarms as a function of the relative cooking time.

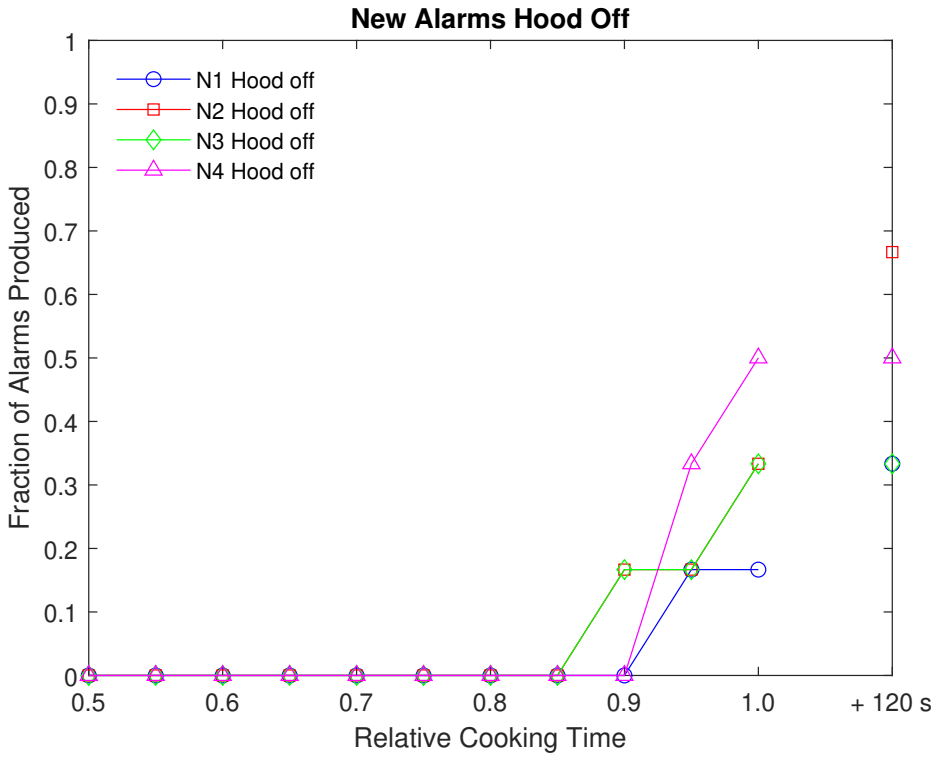

Fig. 19. Fraction of broiling hamburger tests where a smoke alarm signal was produced for the new smoke alarms as a function of the relative cooking time, with the range hood off.

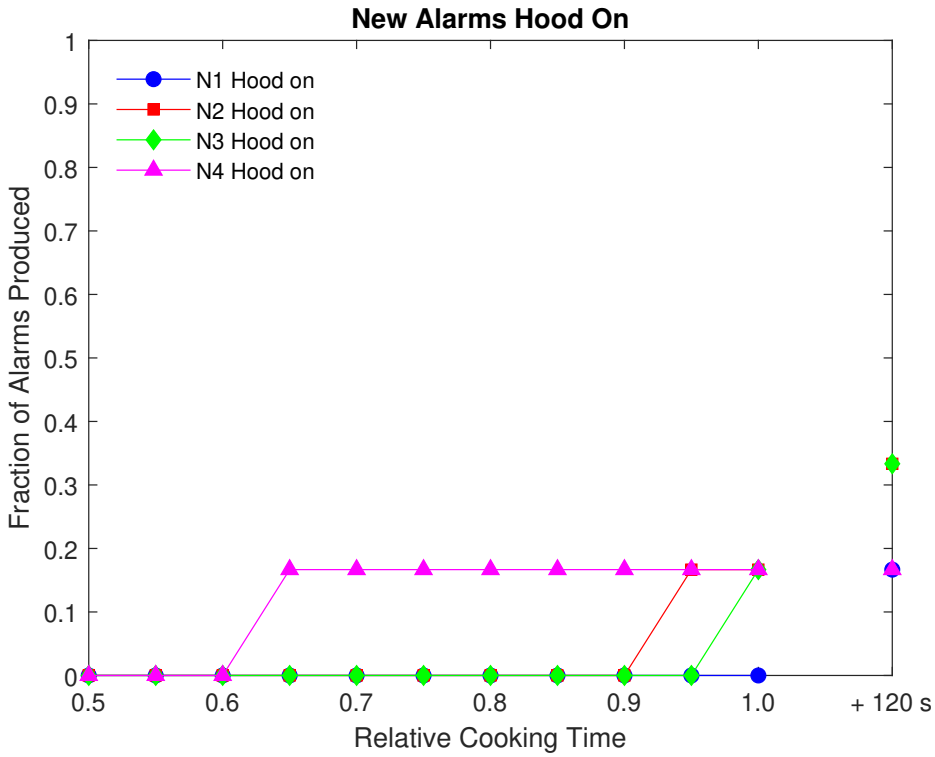

Fig. 20. Fraction of broiling hamburger tests where a smoke alarm signal was produced for the new smoke alarms as a function of the relative cooking time, with the range hood on.

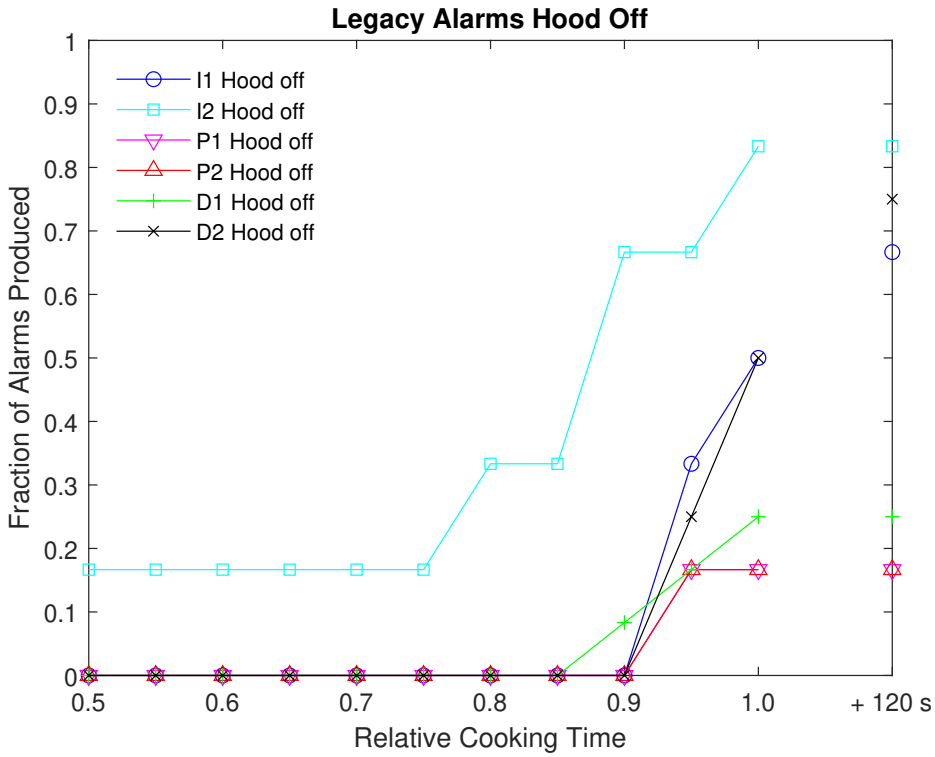

Fig. 21. Fraction of broiling hamburger tests where a smoke alarm signal was produced for the legacy smoke alarms as a function of the relative cooking time, with the range hood off.

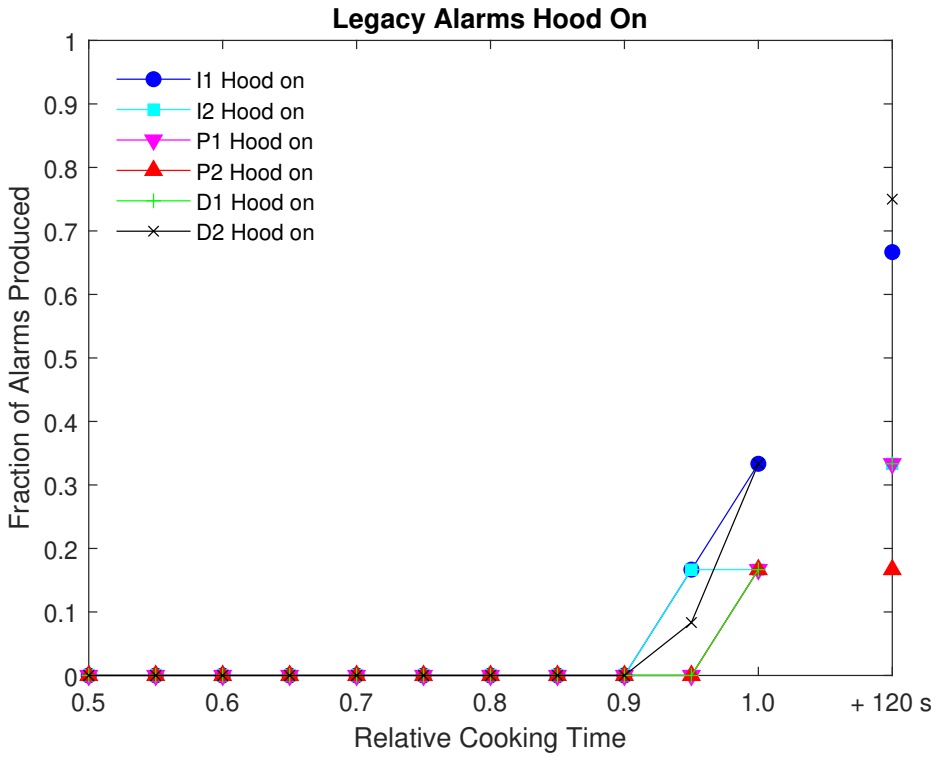

Fig. 22. Fraction of broiling hamburger tests where a smoke alarm signal was produced for the legacy smoke alarms as a function of the relative cooking time, with the range hood on.

Because the alarm performance tended to be similar among the same alarm types, the results for broiling hamburgers are also plotted by alarm type in Fig. 23 for hood off and Fig. 24 for hood on. The shaded regions show the standard deviation in performance across the four new alarms. The final fraction of activations for broiling hamburgers within the duration of the cooking plus 120 s for each smoke alarm type is also given in Table 3. For hood off cases, the new alarms on average performed better than legacy ionization alarms, but worse than the legacy photoelectric alarms. The new alarm performance for broiling hamburgers was very similar to the legacy dual-type alarms. With the hood on, all smoke alarm types performed better than with the hood off, and average performance was similar between all types up to the end of cooking time. Considering the 120 s after cooking ended, the legacy ionization and dual-type alarms produced significantly more alarms compared to legacy photoelectric or new alarms with the hood on.

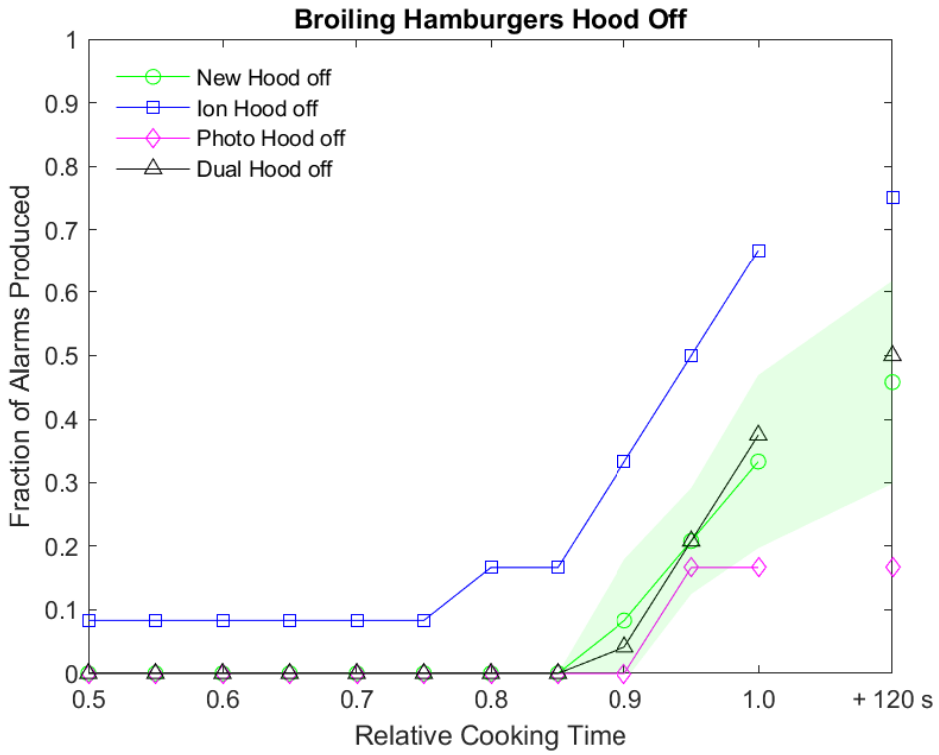

Fig. 23. Fraction of broiling hamburger tests where a smoke alarm signal was produced for each smoke alarm type, on average, as a function of the relative cooking time, with the range hood off. Shaded region shows the standard deviation in performance for the new alarms.

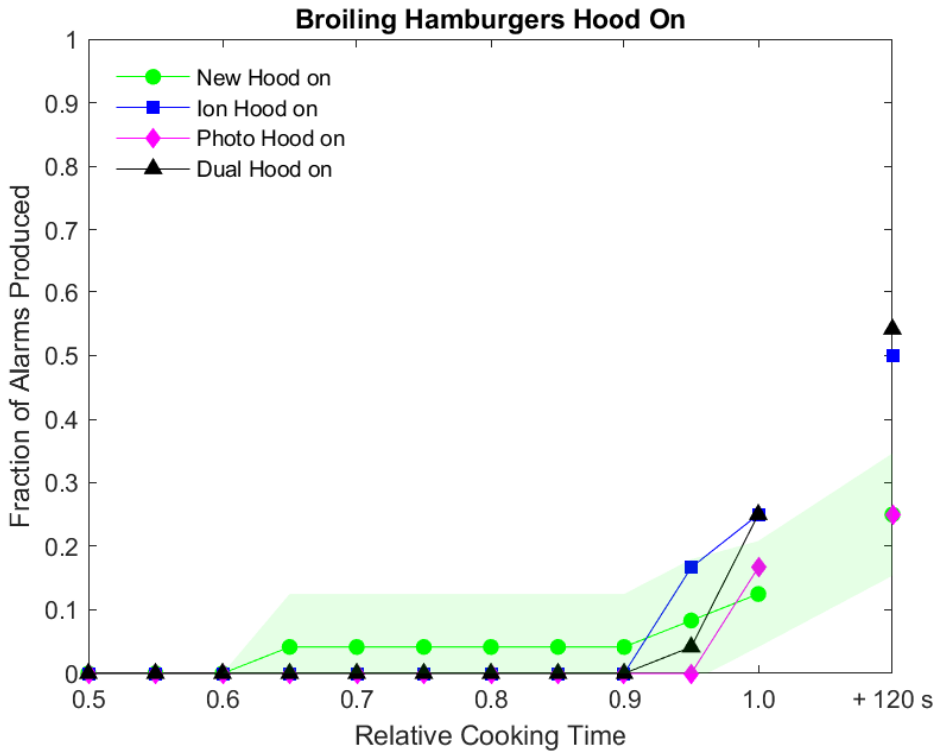

Fig. 24. Fraction of broiling hamburger tests where a smoke alarm signal was produced for each smoke alarm type, on average, as a function of the relative cooking time, with the range hood on. Shaded region shows the standard deviation in performance for the new alarms.

The frying hamburger scenario also caused many alarm signals to be produced, as can be seen in Fig. 25 showing the reference alarms. Again, the reference alarm in location 14 tended to activate earlier and more often than the reference alarm in location 13. The fraction of alarms produced in frying hamburger tests for the new smoke alarms are plotted in Fig. 26 with the range hood off with open symbols and the range hood on with closed symbols. All four new alarms had significant fractions of tests with the range hood off produce an alarm signal the end of the cooking time and significant variability between the new models. There was no change in the fraction of alarms produced in the 120 s following the end of cooking for any of the smoke alarm models. Models N2 and N3 produced the most alarms (83 %) with the hood off, followed by N4 with 67 %, and N1 with 50 %. The tests with the range hood on had noticeably fewer alarm signals, with N2 being the only model producing any alarms (33 %). The new and legacy alarm performance for the frying hamburger scenario is summarized in Figs. 27 and 28 which average the results by alarm type, and the final results are also provided in Table 3. For the frying hamburger tests with hood off, the legacy photoelectric alarms (diamonds) and legacy dual-type alarms (triangles) had the least number of activations (25 % at the end of the test) and performed

essentially the same. The legacy ionization alarms had more activations (58 % at the end of the test) and performed similarly to the average of the new alarms. Turning on the range hood had an especially significant effect to reduce the fraction of activations for the new alarms and the legacy ionization alarms, as shown in Fig. 28. While the legacy photoelectric alarm and legacy dual-type alarm performance was not improved much by turning on the range hood, both of these alarm types had a low fraction of frying hamburger activations with the hood off.

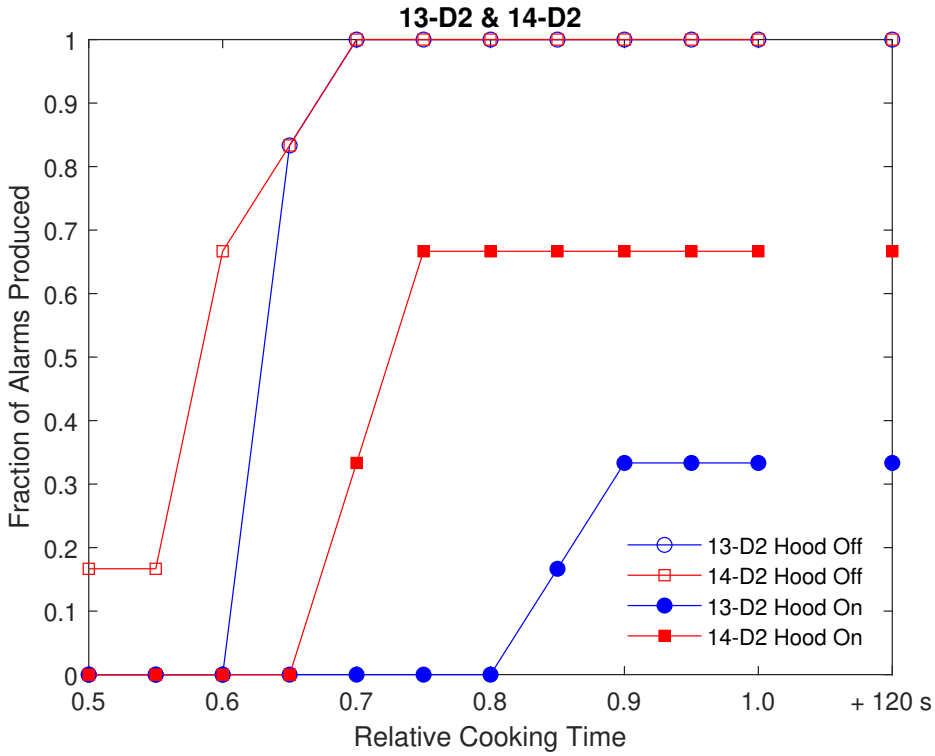

Fig. 25. Fraction of frying hamburger tests where a smoke alarm signal was produced for the reference smoke alarms as a function of the relative cooking time.

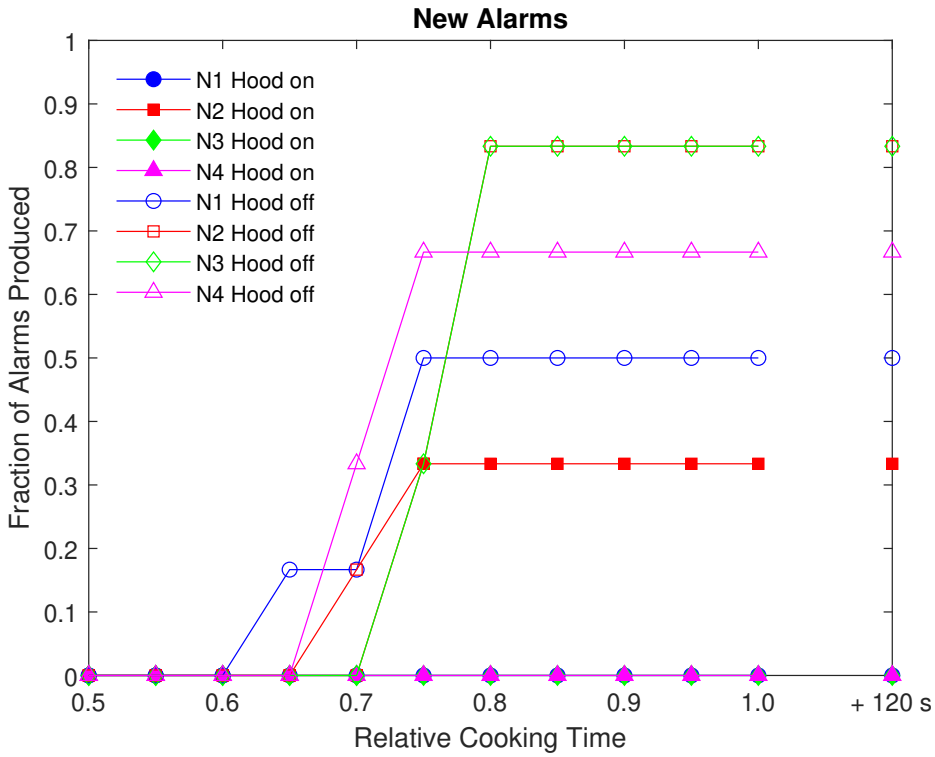

Fig. 26. Fraction of frying hamburger tests where a smoke alarm signal was produced for the new smoke alarms as a function of the relative cooking time, with the range hood off and on.

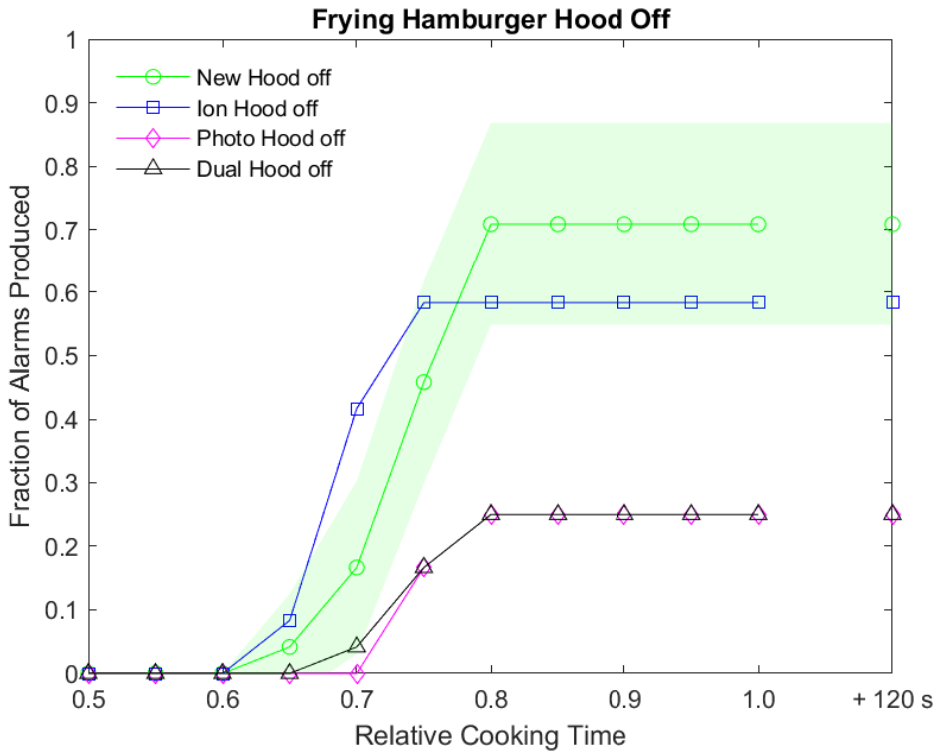

Fig. 27. Fraction of frying hamburger tests where a smoke alarm signal was produced for each smoke alarm type, on average, as a function of the relative cooking time, with the range hood off. Shaded region shows the standard deviation in performance for the new alarms.

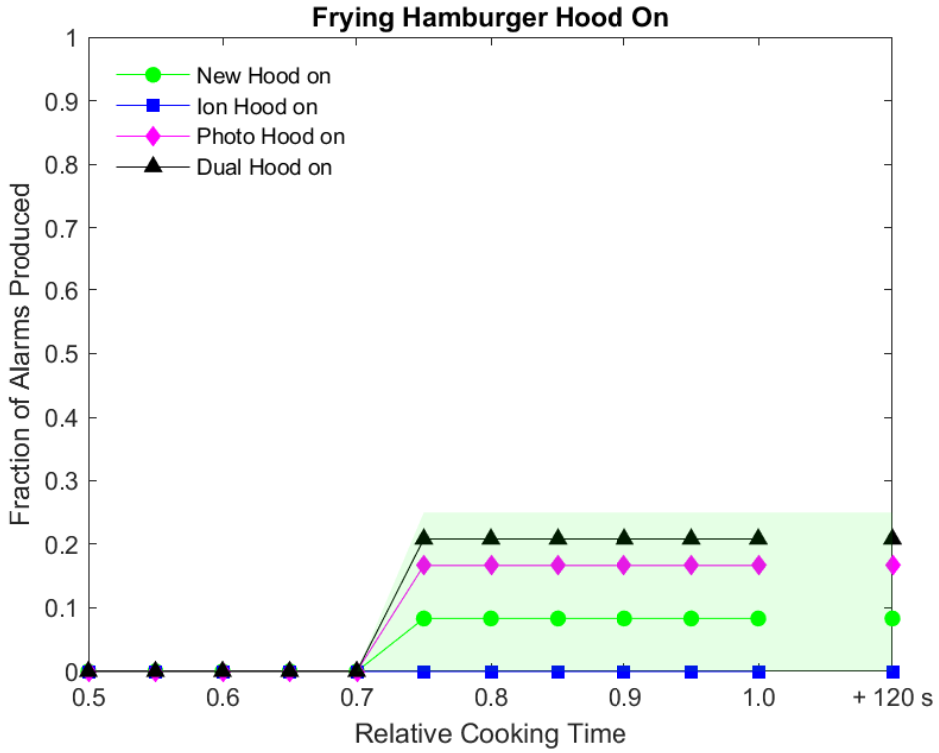

Fig. 28. Fraction of frying hamburger tests where a smoke alarm signal was produced for each smoke alarm type, on average, as a function of the relative cooking time, with the range hood on. Shaded region shows the standard deviation in performance for the new alarms.

The frying bacon scenario produced many alarm signals, notably activating both reference alarms in all tests as shown in Fig. 29. The fraction of activations for new smoke alarms during the frying bacon scenario are shown in Fig. 30 for the hood off and Fig. 31 for the hood on. One observation for frying bacon that applied across the smoke alarms tested, was that many of the alarm signals were produced in the 120 s after the end of cooking. Before the end of cooking time, models N1, N2, and N4 all were activated in at least 50 % of frying bacon tests with the range hood off, and the fraction of N3 alarms was lower at 17 %. However, considering the 120 s after the end of cooking, the fraction of alarms activated increased significantly for all new models. With the range hood on, Fig. 31, there were almost no new alarm activations before the end of cooking; only model N3 had any with 17 %. In the next 120 s, both models N2 and N4 produced alarms, with the fraction of N2 alarms increasing to 67 % for frying bacon with the hood on. Figures 32 and 33 compare the frying bacon scenario performance by alarm type, and the final results are also provided in Table 3. For both hood off and hood on cases there are very few legacy alarms produced before the end of the cooking time. The only legacy alarm activations for the hood off in Fig. 32 are the legacy ionization alarms at 33 %, and the only legacy alarm

activations for the hood on in Fig. 33 are the legacy dual-type alarms at 17 %. However the average performance is very similar among all legacy alarm types as well as new alarms when considering alarms produced in the 120 s after the end of cooking time for frying bacon. With the range hood off (Fig. 32), both new alarms and legacy ionization alarms produced some signals before the end of cooking, and often many of the other alarms were activated eventually. With the range hood on, the new alarms and legacy ionization alarms actually had a lower fraction of alarms activated compared to the legacy photoelectric and dual-type alarms, considering the 120 s after the end of cooking.

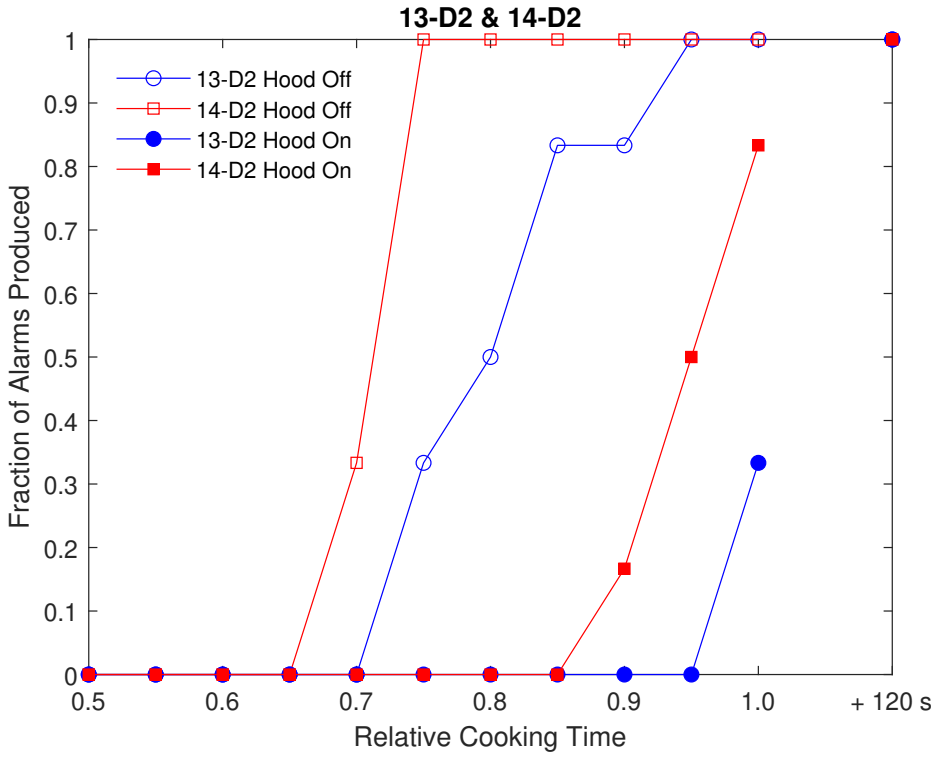

Fig. 29. Fraction of frying bacon tests where a smoke alarm signal was produced for the reference smoke alarms as a function of the relative cooking time.

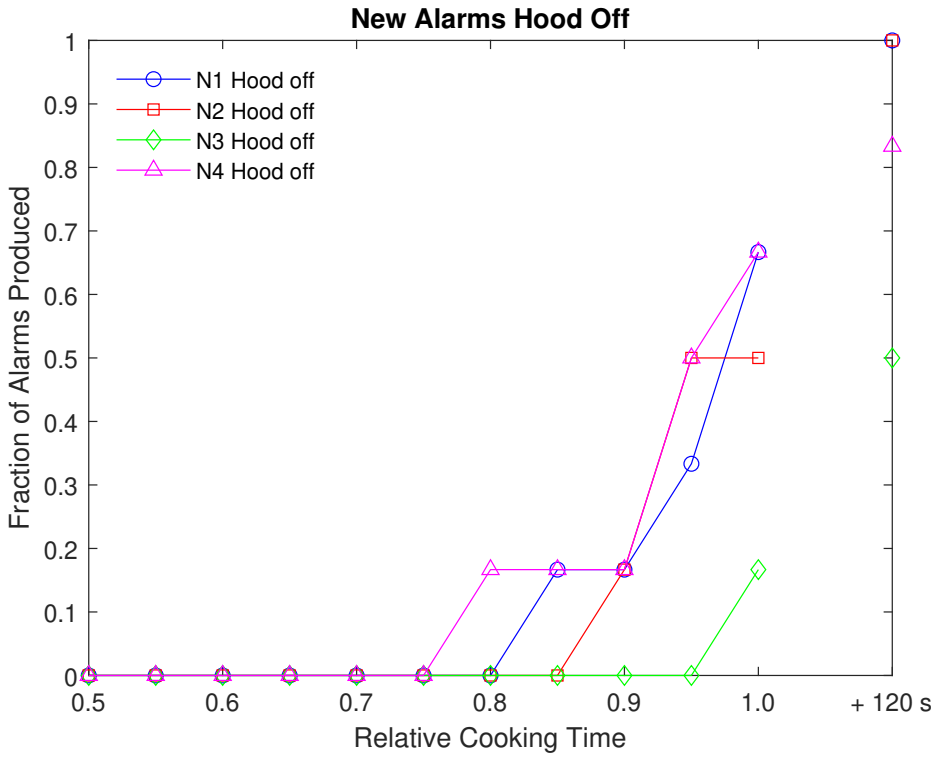

Fig. 30. Fraction of frying bacon tests where a smoke alarm signal was produced for the new smoke alarms as a function of the relative cooking time, with the range hood off.

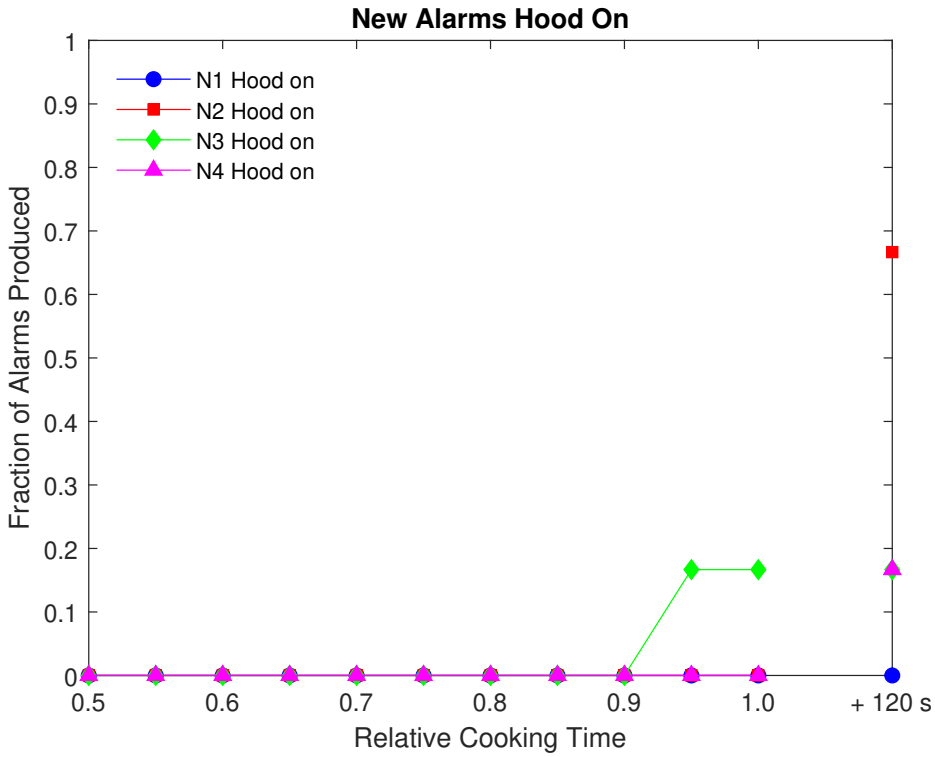

Fig. 31. Fraction of frying bacon tests where a smoke alarm signal was produced for the new smoke alarms as a function of the relative cooking time, with the range hood on.

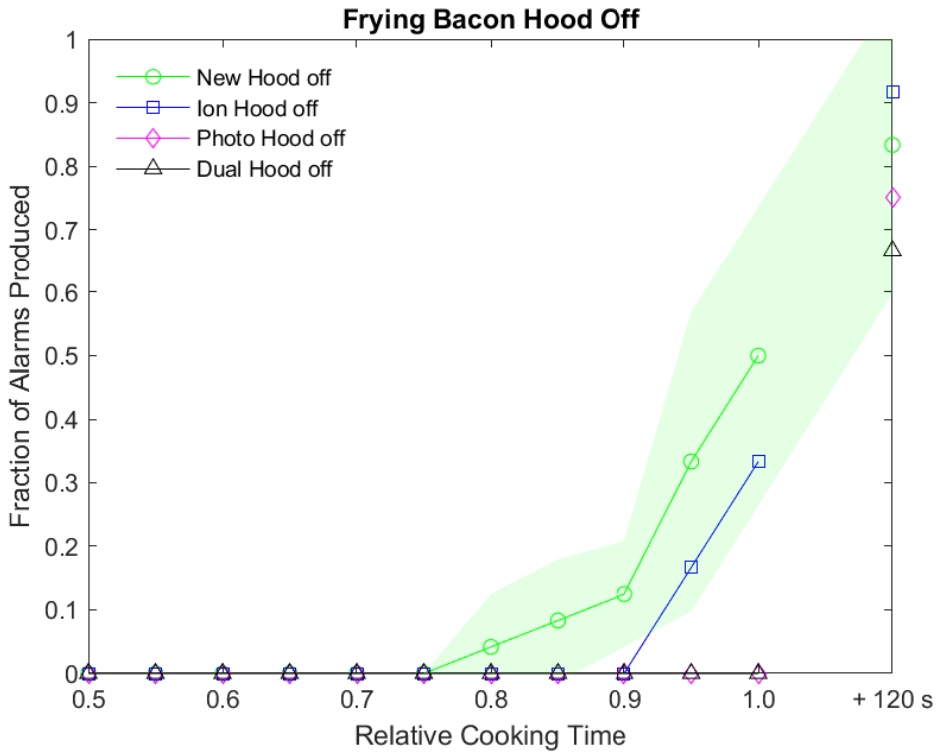

Fig. 32. Fraction of frying bacon tests where a smoke alarm signal was produced for each smoke alarm type, on average, as a function of the relative cooking time, with the range hood off. Shaded region shows the standard deviation in performance for the new alarms.

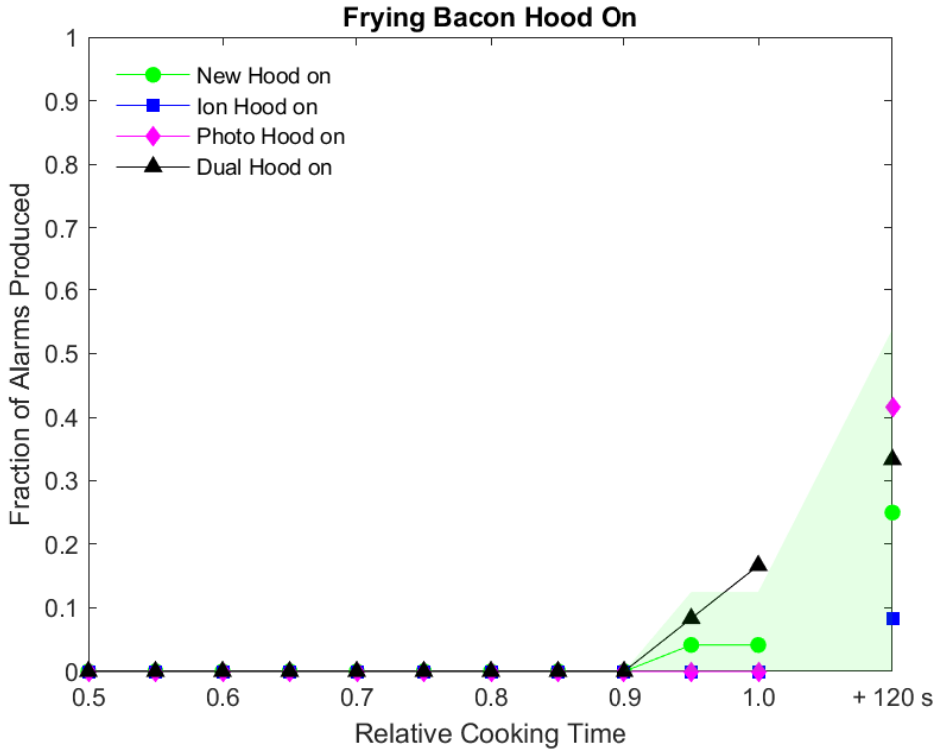

Fig. 33. Fraction of frying bacon tests where a smoke alarm signal was produced for each smoke alarm type, on average, as a function of the relative cooking time, with the range hood on. Shaded region shows the standard deviation in performance for the new alarms.

The dark toast scenario was expected to be challenging for any smoke alarms that use ionization chambers, as was previously observed in Cleary [2]. Both reference alarms, which were dual ionization and photoelectric type alarms, were activated in all dark toast tests as shown in Fig. 34. From the new alarm performance in Fig. 35, it can be seen that only models N1 and N4 were activated in dark toast tests, and therefore presumably N1 and N4 employ some type of ionization technology. Model N4 was activated in all dark toast tests with the hood off, and a third of the tests with the hood on. Model N1 had fewer alarms during the cooking time, but produced alarms in all tests with the hood off considering the additional 120 s. With the hood on, model N1, did not produce any alarms. Models N2 and N3 were not activated in any dark toasts and presumably did not use ionization technology. Figures 36 and 37 show the fraction of activations by alarm type during dark toast tests, and the final results are also provided in Table 3. Both legacy ionization alarms were activated in all dark toast tests with the range hood off when considering the cooking time plus 120 s. The large shaded region in Figure 36 represents the standard deviation in performance among the new alarms, which demonstrates significant differences due to the use of ionization technology. On average the new alarms and legacy dual-type alarms

produced an alarm in about half of the dark toast tests. For the new alarms, this was a result of some alarm models activating and other alarm models never activating during dark toast tests. With the range hood on, the fractions of tests with an alarm signal were significantly lower, suggesting the additional airflow was effective at diluting the toasting bread aerosols. The legacy photoelectric alarms never produced a signal in any of the dark toast tests.

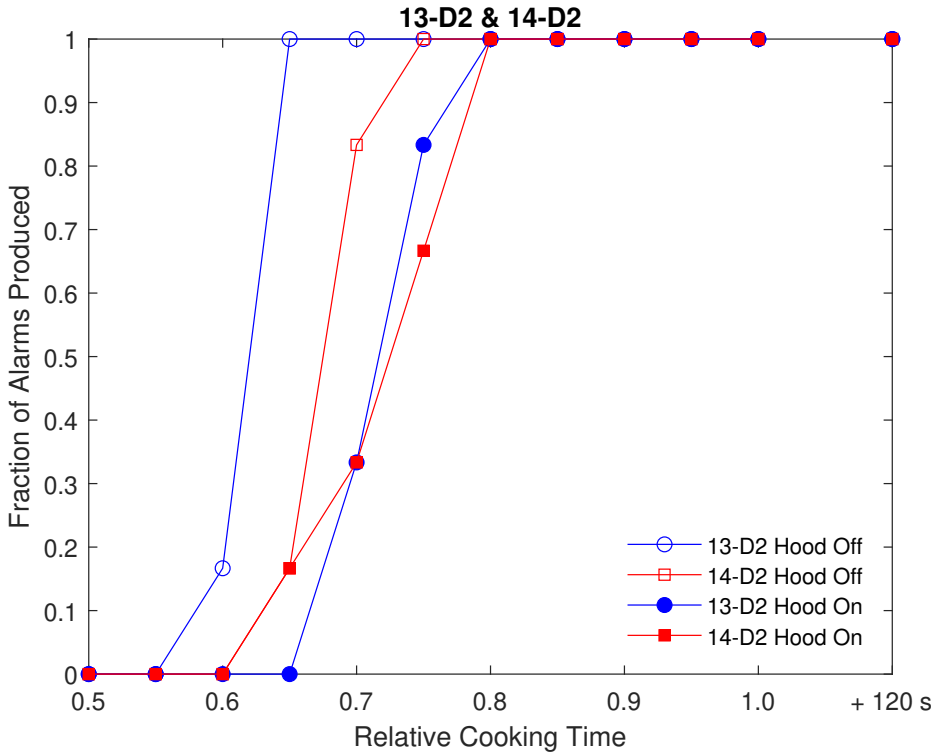

Fig. 34. Fraction of dark toast tests where a smoke alarm signal was produced for the reference smoke alarms as a function of the relative cooking time.

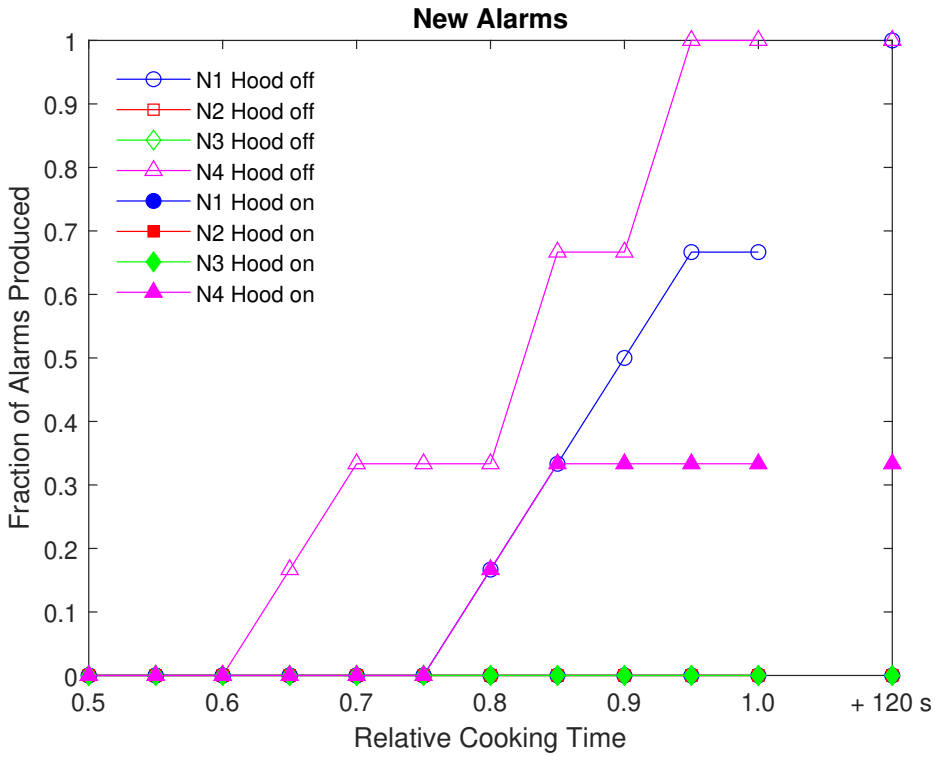

Fig. 35. Fraction of dark toast tests where a smoke alarm signal was produced for the new smoke alarms as a function of the relative cooking time, with the range hood off and on.

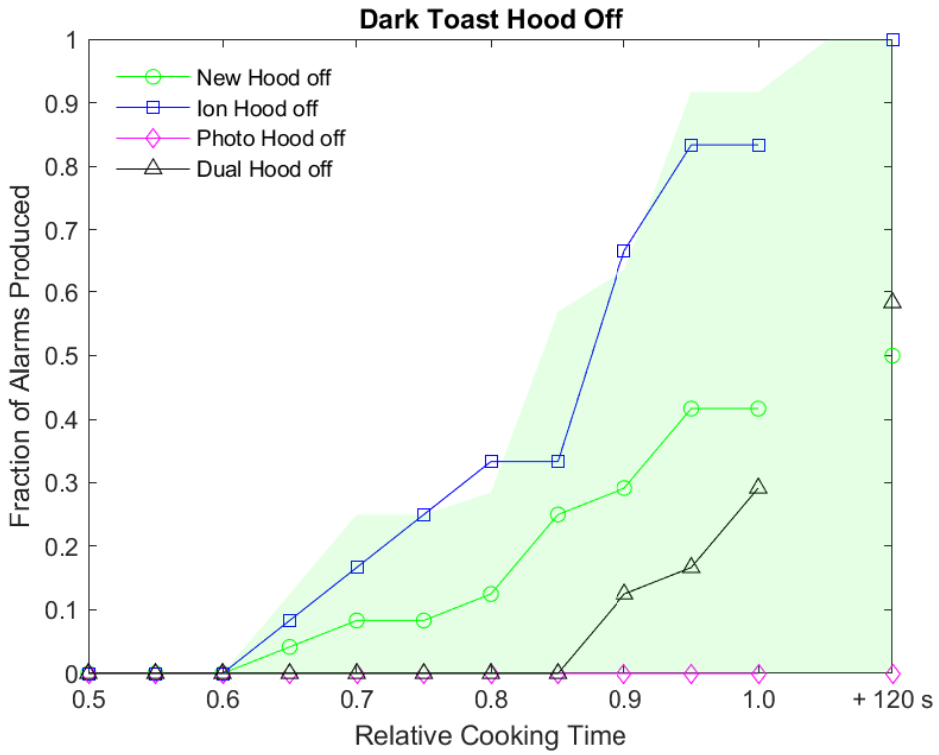

Fig. 36. Fraction of dark toast tests where a smoke alarm signal was produced for each smoke alarm type, on average, as a function of the relative cooking time, with the range hood off.

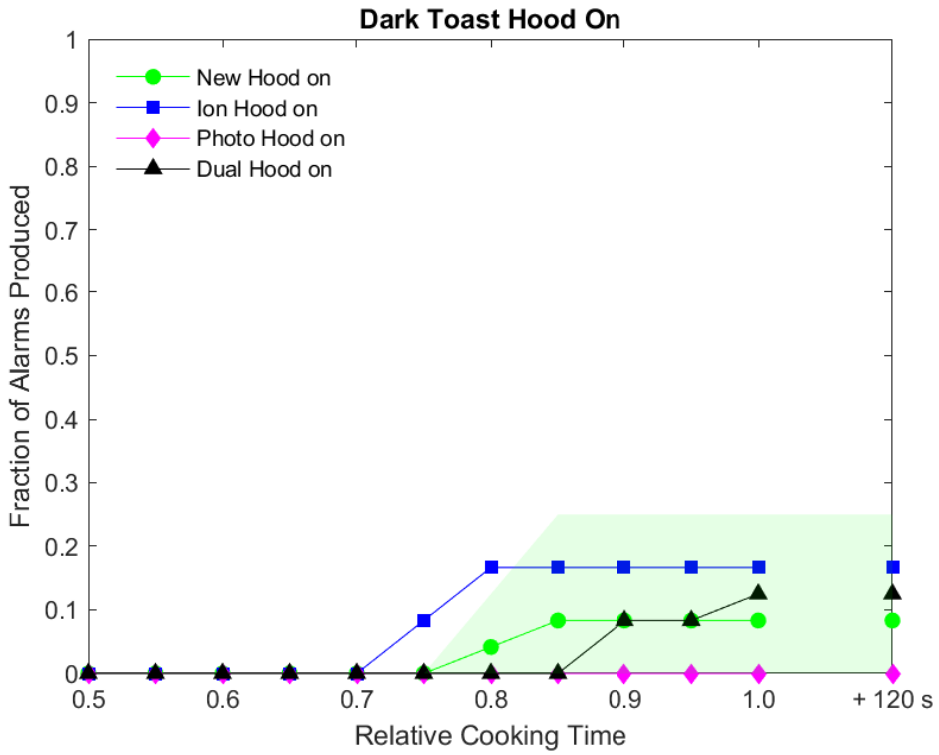

Fig. 37. Fraction of dark toast tests where a smoke alarm signal was produced for each smoke alarm type, on average, as a function of the relative cooking time, with the range hood on.

The overall performance, averaged across all cooking scenarios and grouped by alarm type, is given at the bottom of Table 3. The overall values in Table 3 are an average of the overall performance for individual alarm models in Table 2, which can be referenced for the range in performance among different models of the same alarm type. The new alarms, as a group, show slightly better performance than legacy ionization alarms, but not better than legacy photoelectric or dual-type alarms. With the range hood off, the legacy photoelectric alarms were activated in the lowest fraction of tests (12 %), while the new alarms were activated for 31 %. With the range hood on, the new alarms and legacy photoelectric alarms were activated in the same fraction of tests (8 %).

3.2. Aerosol Results

The following section discusses the number and mass concentration, diameter concentration (total aerosol length), and mass mean diameter of the particles created by the various cooking scenarios.

During the broiling hamburgers scenario tests, the relative humidity in the room decreased as the room temperature increased as shown in the data from one test with the range hood

off in Fig. 38 where the humidity decreased by 8.9 % while the temperature increased 5.9 °C. Figure 39 shows an example of the mass concentration and mass mean diameter during a typical broiling hamburgers test with the range hood off. Note that the concentration and diameter measurements are not shown from the start of cooking time to 200 s, when the concentrations were very low and oscillated due to noise. In general, the mass concentration increased while the heat source was on then decreased in the last two minutes of data collection after the heat source was turned off. During the first 1000 s of cooking in Fig. 39, both the mass concentration and the mass mean diameter stayed relatively low, then both increased rapidly after 1000 s before leveling off and dropping after 1200 s. The alarms that were produced all activated during the rapid increase as shown by the various symbols on the mass concentration curve. In Fig. 40, the alarm activations also coincided with a significant increase in the diameter concentration, which is the total aerosol length per unit volume and the first moment of the number concentration measurement. The diameter concentration is a measure of total length of particles, if the particles were lined up end to end, per unit volume. The sensitivity of ionization smoke detectors has been correlated with aerosol diameter concentration [7]. Just before all the alarm activations, the number concentration decreased, also shown in Fig. 40.

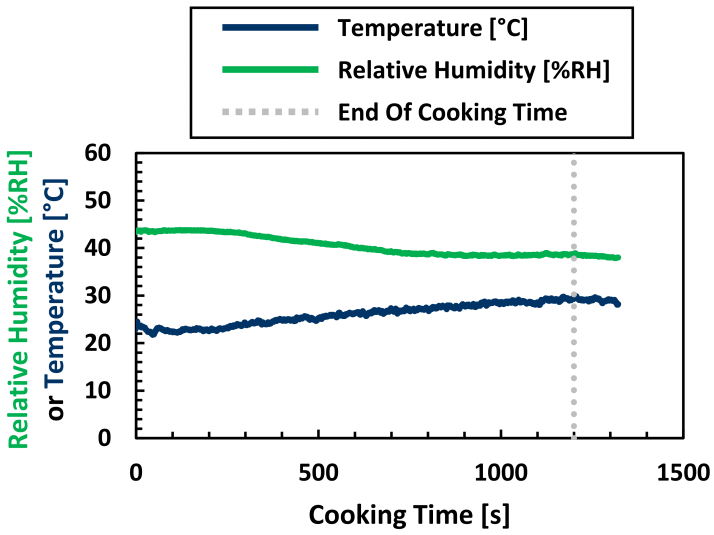

Fig. 38. The relative humidity and temperature at the ceiling for a typical broiling hamburgers test over the cooking time.

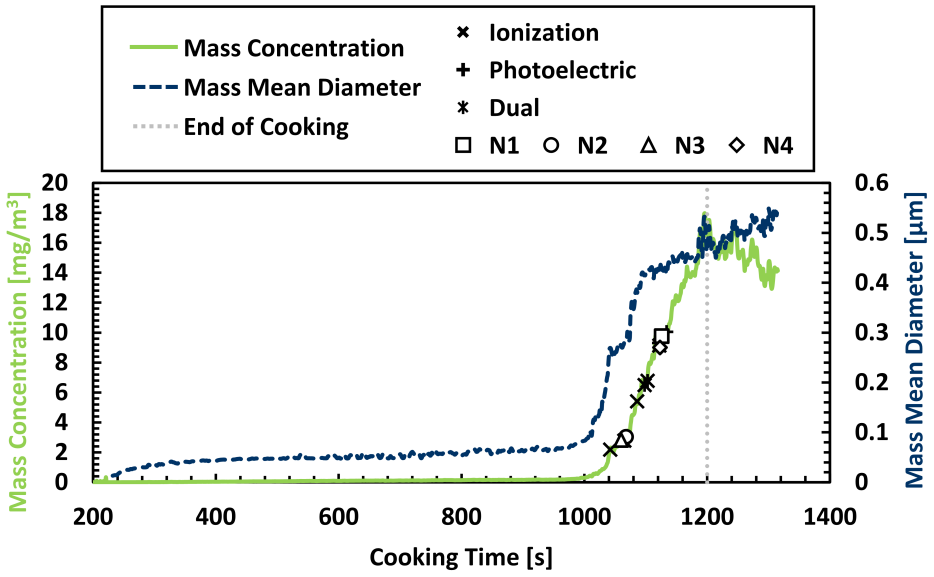

Fig. 39. The mass concentration and the mass mean diameter over the cooking time of a typical broiling hamburgers test. Symbols indicate when alarm activated and the mass concentration at activation.

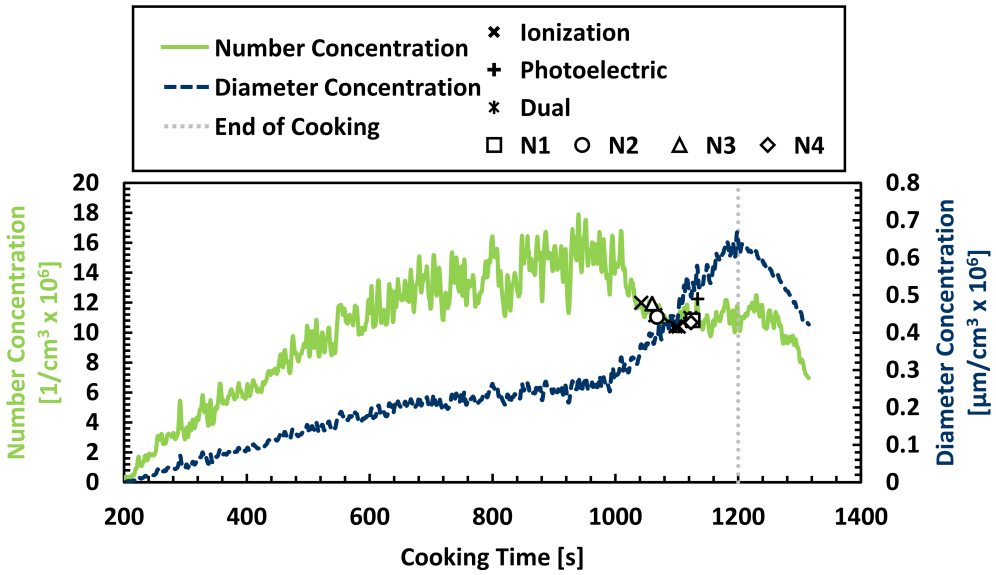

Fig. 40. The number concentration and the diameter concentration over the cooking time of a typical broiling hamburgers test. Symbols indicate when alarm activated and the number concentration at activation.

Figure 41 shows the mass concentration at the time of alarm for the new alarms during the broiling hamburgers tests with both the hood on and the hood off. If the alarm did not

activate during a given test, the maximum mass concentration during that test is shown with an open circle. The mass concentration at alarm was generally similar for hood off and hood on and across all four new alarm models, with an average value of 3.0 mg/m^3. Many of the tests with no alarm had maximum mass concentrations at or below this level. Figure 42 similarly shows the beam obscuration at the time of alarm or the maximum obscuration during each of the broiling hamburgers tests. The average beam obscuration at alarm was 1.21 %/ft. Generally, the beam obscuration maximum was about 1.5 %/ft or less for the tests where a particular alarm model did not activate.

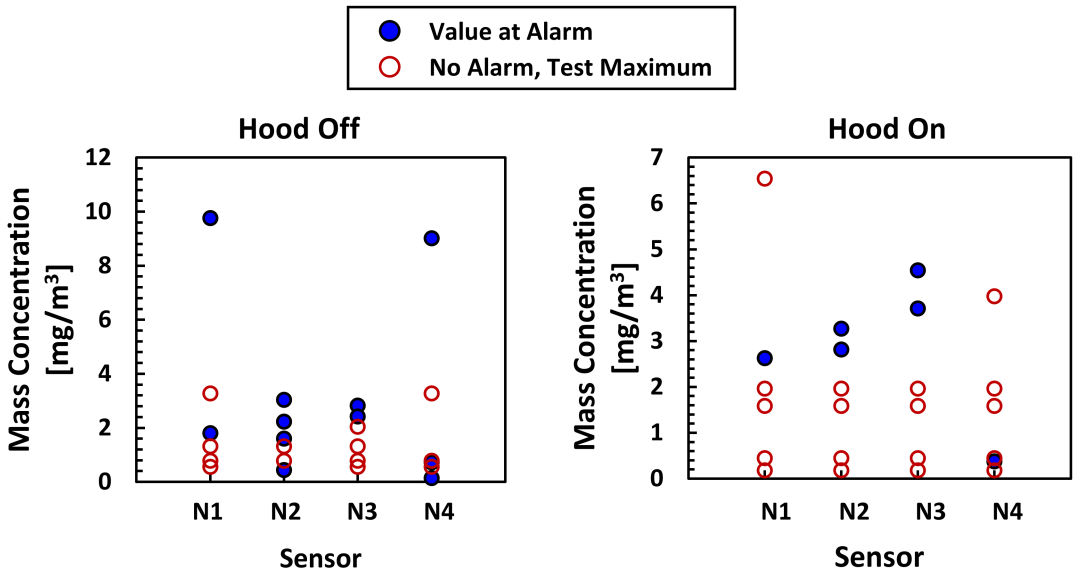

Fig. 41. Mass concentration at time of alarm (closed symbols) or at maximum mass concentration if no alarm (open symbols) for the N1, N2, N3, and N4 alarms with the hood off (left) and the hood on (right) for the broiling hamburgers tests.

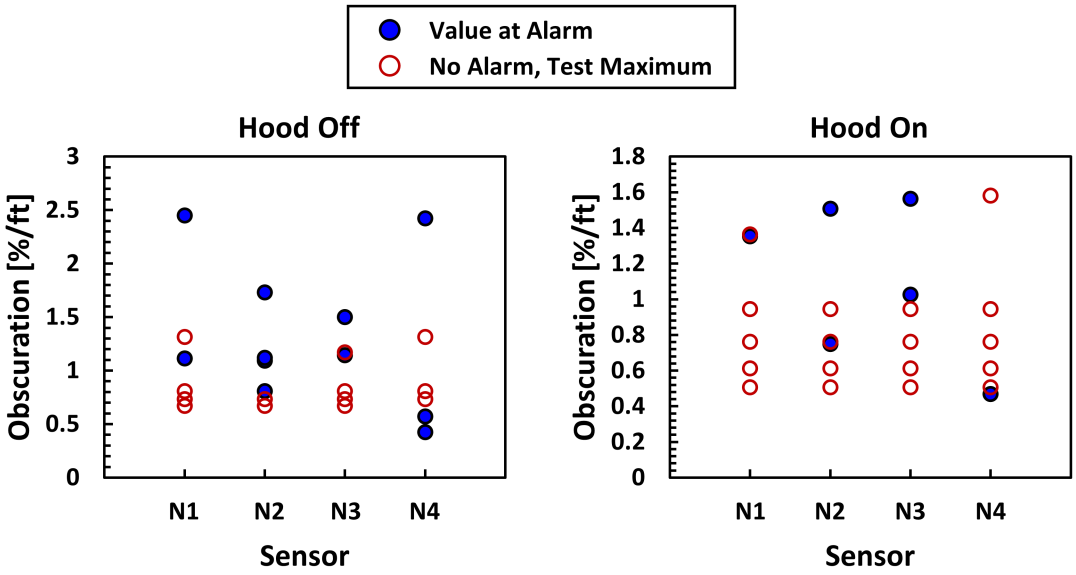

Fig. 42. Beam obscuration at time of alarm (closed symbols) or at maximum obscuration if no alarm (open symbols) for the N1, N2, N3, and N4 alarms with the hood off (left) and the hood on (right) for all broiling hamburgers tests.

The other cooking scenario that used the oven was frozen pizza. Figure 43 shows the mass concentration and mass mean diameter for a typical frozen pizza test. The mass concentration and mass mean diameter do not have a period of rapid increase as seen in Fig. 39 for the broiling hamburgers, and the maximum values in Fig. 43 are similar to the first 1000 s of the broiling hamburgers (Fig. 39). Only one new alarm, N4, activated in this test. Figure 44 shows the number concentration and the diameter concentration throughout the pizza test. Figure 45 shows the mass concentration at alarm for the new alarms or the maximum concentration during the test if the alarm did not activate. The frozen pizza scenario generated maximum mass concentration values up to 1.6 mg/m^3, considerably less than the broiling hamburgers scenario. Consequently, there were only two activations of new smoke alarms across all frozen pizza tests.

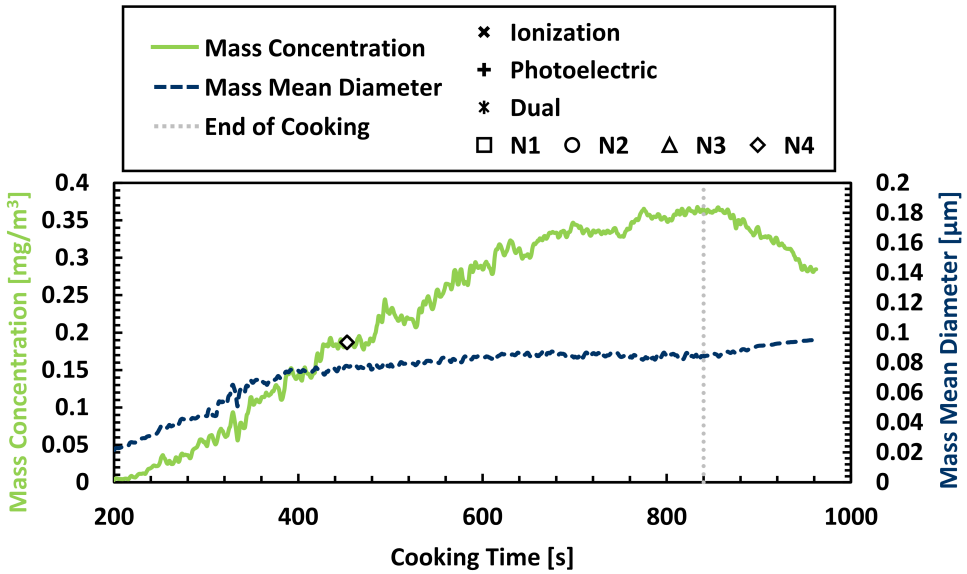

Fig. 43. The mass concentration and the mass mean diameter over the cooking time of a typical frozen pizza test. Symbols indicate when alarm activated and the mass concentration at activation.

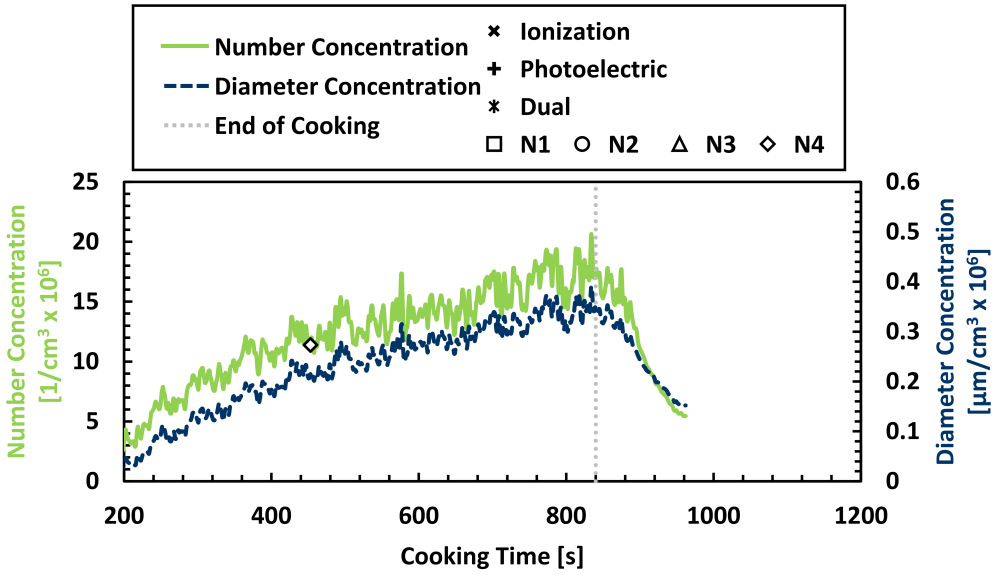

Fig. 44. The number concentration and the diameter concentration over the cooking time of a typical frozen pizza test. Symbols indicate when alarm activated and the number concentration at activation.

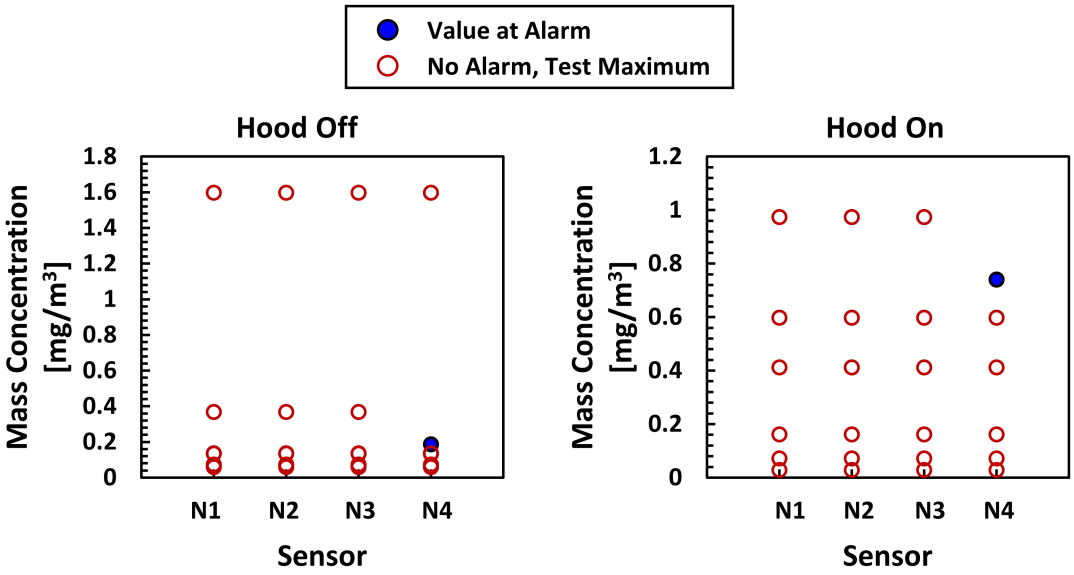

Fig. 45. Mass concentration at time of alarm (closed symbols) or at maximum mass concentration if no alarm (open symbols) for the N1, N2, N3, and N4 alarms with the hood off (left) and the hood on (right) for all frozen pizza tests.

The toasting scenarios also produced small particles similar to the oven scenarios. The mass concentration and mass mean diameter for a typical regular toast test is shown in Fig. 46, along with the activation time of any smoke alarms. Only one legacy ionization alarm and one new alarm (N4) was activated in this particular test shown in Fig. 46. The mass mean diameter is relatively flat throughout the scenario, around 0.08 μm, and similar to the size of particles produced in the beginning of the broiling hamburgers test and throughout the frozen pizza test. Figure 47 shows the number concentration and the diameter concentration throughout the same regular toast test. The mass and number concentrations increases up to around 180 s, the end of cooking, and a couple of smoke alarms activated afterward. Figure 48 shows the mass concentration at alarm for the N1, N2, N3, and N4 alarms or the maximum concentration during the test if the alarm did not activate. Of the new alarms, only models N1 and N4 were activated in regular toast tests, and only when the range hood was off when the maximum mass concentration was significantly higher.

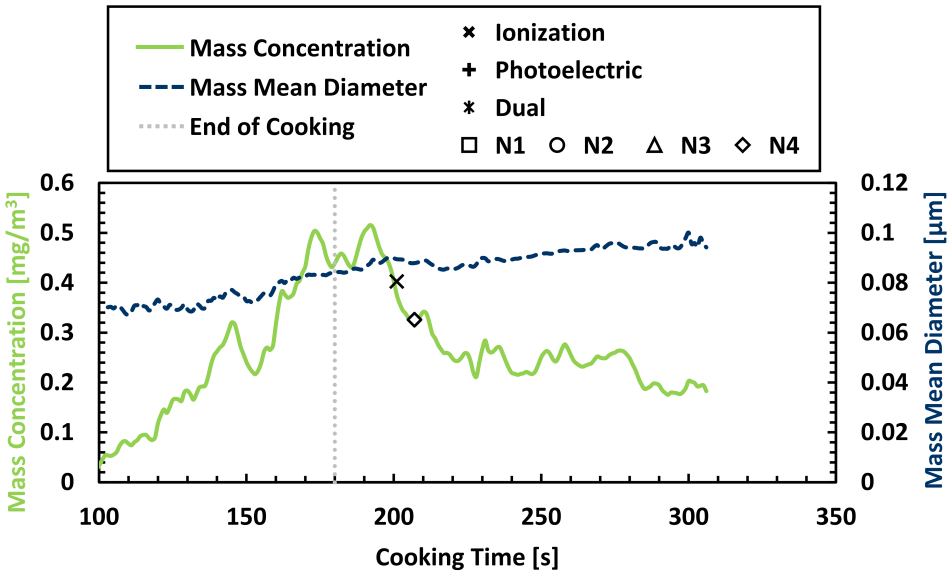

Fig. 46. The mass concentration and the mass mean diameter over the cooking time of one of a typical regular toast test. Symbols indicate when alarm activated and the mass concentration at activation.

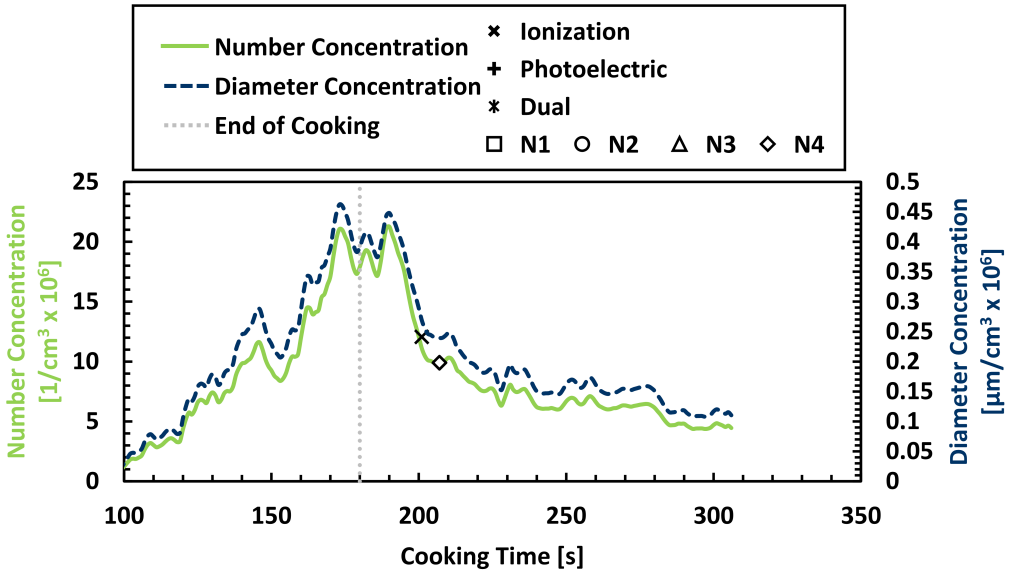

Fig. 47. The number concentration and the diameter concentration over the cooking time of one of a typical regular toast test. Symbols indicate when alarm activated and the number concentration at activation.

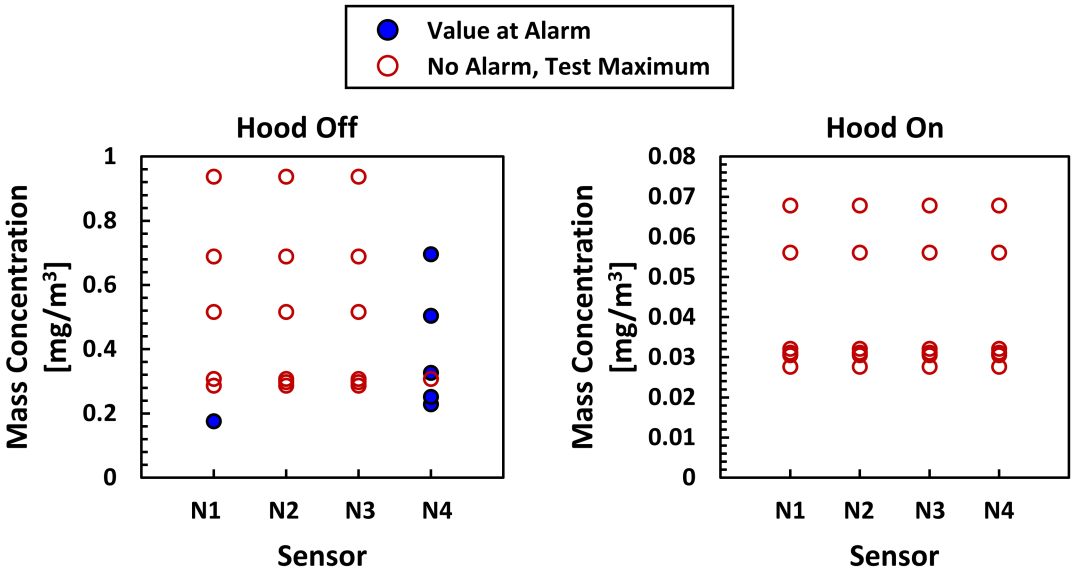

Fig. 48. Mass concentration at time of alarm (closed symbols) or at maximum mass concentration if no alarm (open symbols) for the N1, N2, N3, and N4 alarms with the hood off (left) and the hood on (right) for all regular toast tests.

Figure 49 shows the mass concentration and mass mean diameter for a typical dark toast test. The cooking time for the dark toast scenario was 240 s, which produced particles with slightly greater mass mean diameters than the regular toast, up to about 0.15 μm. Several smoke alarms were activated during the dark toast test as shown in Fig. 49, including legacy ionization, legacy dual-type, and new alarms. Figure 50 shows the number concentration and the diameter concentration throughout the same dark toast test. Figure 51 shows the mass concentration at alarm for the new alarms or the maximum concentration during the test if the alarm did not activate. For the new alarms, only models N1 and N4 activated during dark toast tests. Compared to the regular toast, there were more activations and the maximum mass concentrations tended to be higher as a result of toasting for an extra minute.

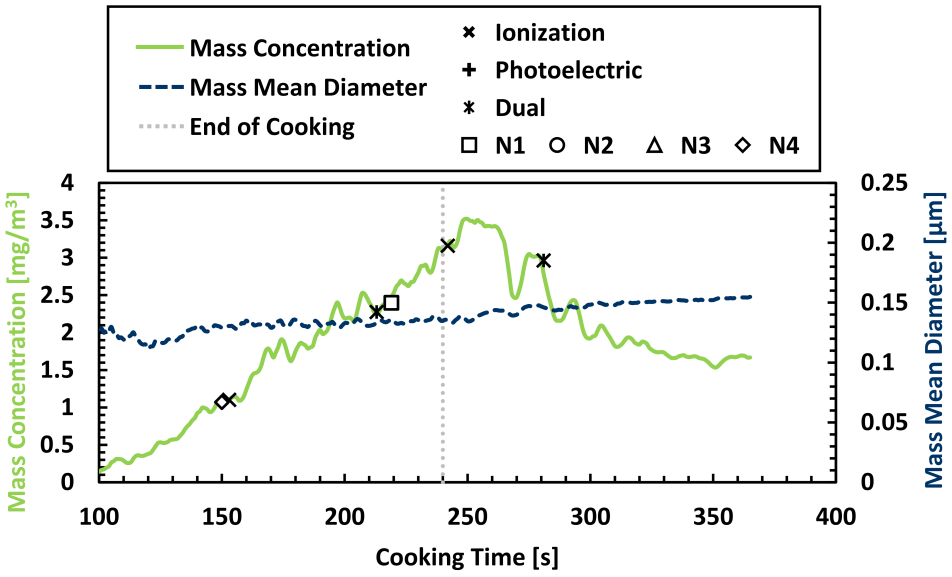

Fig. 49. The mass concentration and the mass mean diameter over the cooking time of one of the dark toast scenarios. Symbols indicate when alarm activated and the mass concentration at activation.

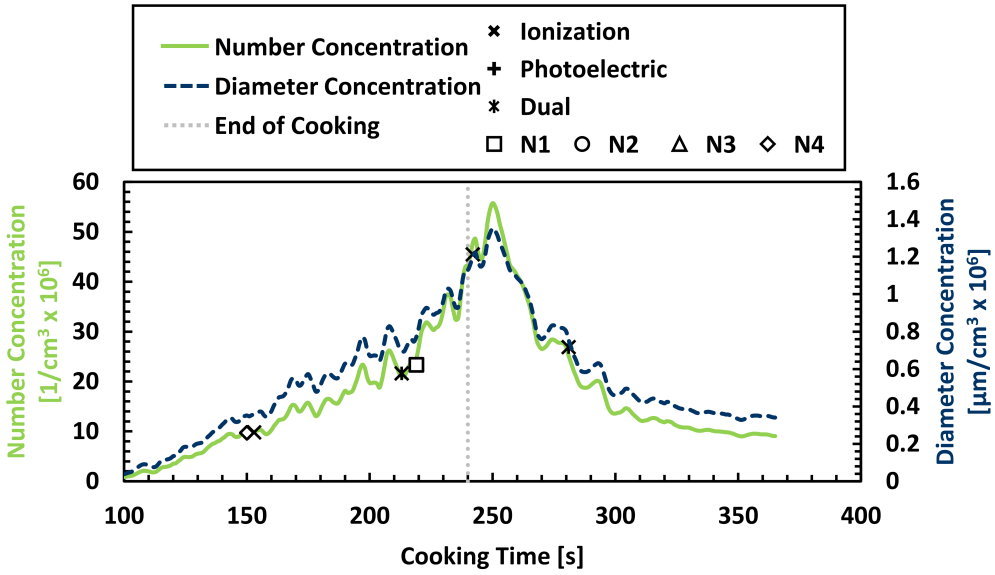

Fig. 50. The number concentration and the diameter concentration over the cooking time of one of the dark toast scenarios. Symbols indicate when alarm activated and the number concentration at activation.

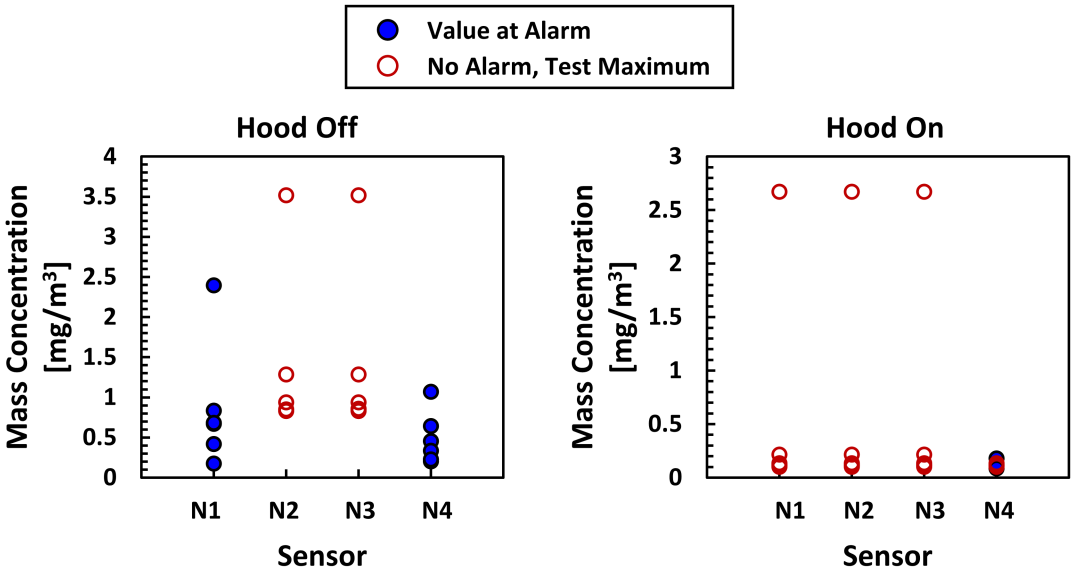

Fig. 51. Mass concentration at time of alarm (closed symbols) or at maximum mass concentration if no alarm (open symbols) for the N1, N2, N3, and N4 alarms with the hood off (left) and the hood on (right) for all dark toast tests.

The toaster was also used to toast the toaster pastries. The mass concentration and mass mean diameter in Fig. 52 and number concentration and diameter concentration in Fig. 53 are very similar to the measurements for regular toast in Figs. 46 and 47, which had the same cooking time, 180 s. No smoke alarms, legacy or new, were activated in this particular toaster pastries test. Figure 54 shows the mass concentration at alarm for the new alarms or the maximum concentration during the test if the alarm did not activate. Like the other toasting tests, only models N1 and N4 activated in a few tests, and for toaster pastries, the activations were limited to tests with the range hood off when the mass concentration was higher.

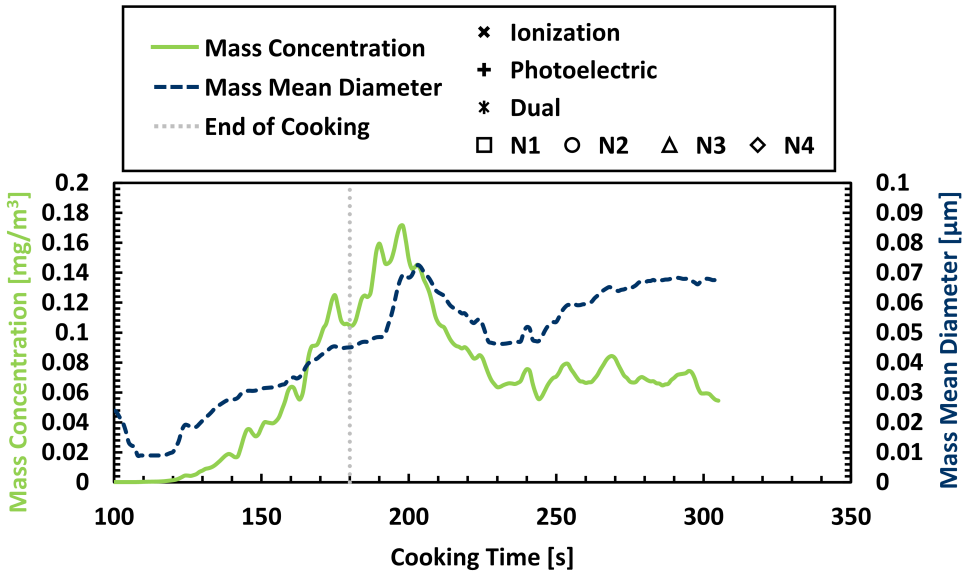

Fig. 52. The mass concentration and the mass mean diameter over the cooking time of one of the toaster pastries tests. No smoke alarms activated during this particular test.

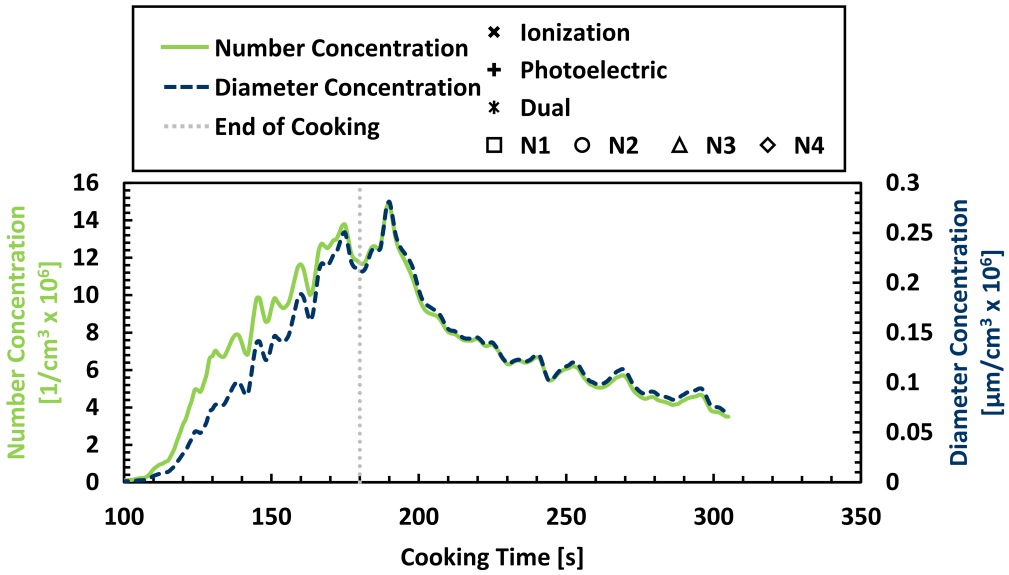

Fig. 53. The number concentration and the diameter concentration over the cooking time of one of the toaster pastries tests. No smoke alarms activated during this particular test.

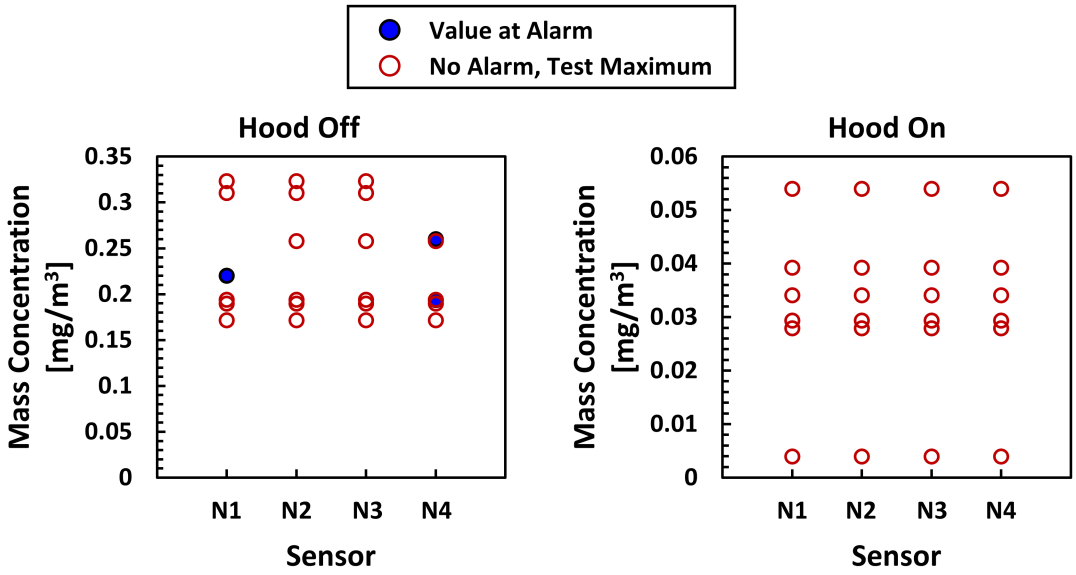

Fig. 54. Mass concentration at time of alarm (closed symbols) or at maximum mass concentration if no alarm (open symbols) for the N1, N2, N3, and N4 alarms with the hood off (left) and the hood on (right) for all toaster pastries tests.

Next is the frying bacon scenario, heated on the cooktop. Figure 55 shows the mass concentration and the mass mean diameter over time of a representative frying bacon test. Figure 56 shows the number concentration and the diameter concentration over time of the same test. All four variables increase over the time the bacon is cooking. The bacon was flipped after 300 s, and then around 400 s, the mass concentration increases at a greater rate than earlier in the test. On average the maximum mass concentration from the bacon cooking scenario was 5.2 mg/m^3 with an average maximum mass mean diameter of 6.8 μm.

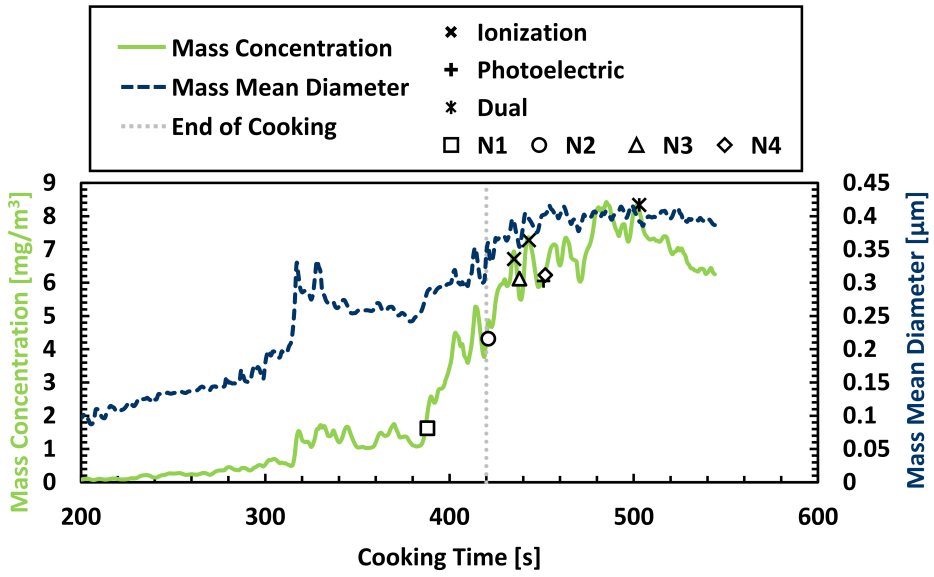

Fig. 55. The mass concentration and the mass mean diameter over the cooking time of a typical frying bacon test. Symbols indicate when alarm activated and the mass concentration at activation.

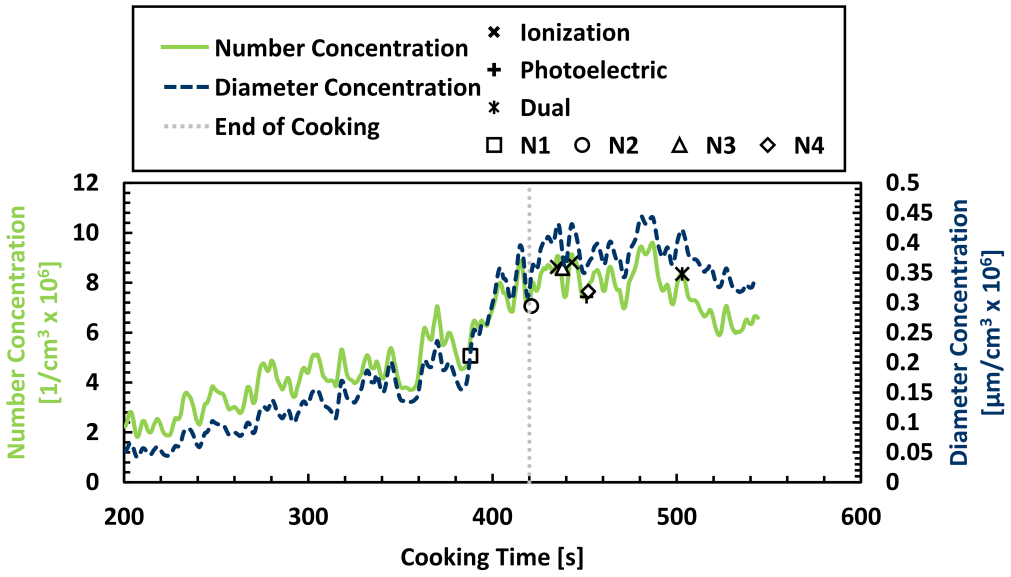

Fig. 56. The number concentration and the diameter concentration over the cooking time of a typical frying bacon test. Symbols indicate when alarm activated and the number concentration at activation.

Figure 57 shows the mass concentration at the time of alarm for the new alarms during the frying bacon tests or the maximum mass concentration during that test if there was no

alarm. The average mass concentration at alarm was 5.7 mg/m^3 with the hood off. With the hood on the average mass concentration at alarm was lower, 2.6 mg/m^3, and there were many tests with no alarm and higher peak mass concentration values. The beam obscuration values at the time of alarm in Figure 58 were also different by about a factor of 2, 1.5 %/ft with the hood off and 0.8 %/ft with the hood on.

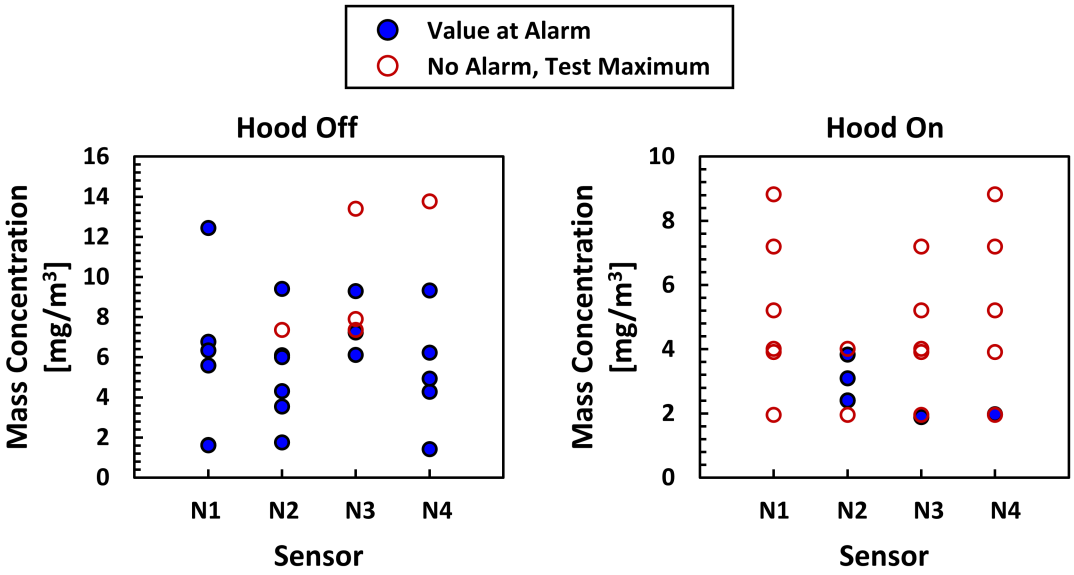

Fig. 57. Mass concentration at time of alarm (closed symbols) or at maximum mass concentration if no alarm (open symbols) for the N1, N2, N3, and N4 alarms with the hood off (left) and the hood on (right) for all frying bacon tests.

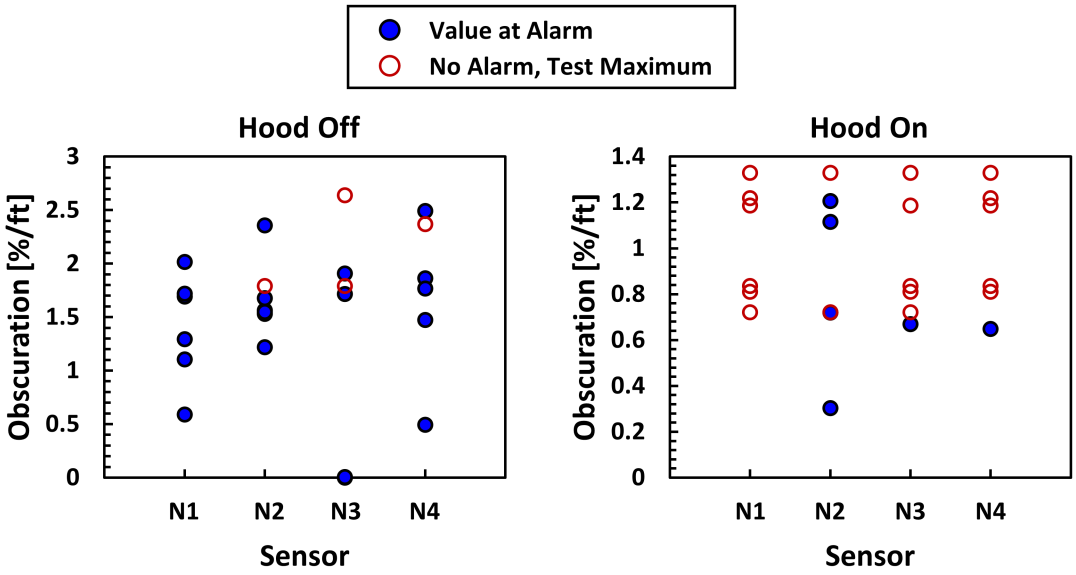

Fig. 58. Beam obscuration at time of alarm (closed symbols) or at maximum obscuration if no alarm (open symbols) for the N1, N2, N3, and N4 alarms with the hood off (left) and the hood on (right) for all frying bacon tests.

The last sets of aerosol measurements are for scenarios where food was heated on the standalone burner. First is the frying hamburger scenario, which generated aerosols sufficient to activate smoke alarms. The mass concentration and mass mean diameter for a typical frying hamburger test is shown in Fig. 59. The mass concentration peaks around 430 s into the cooking time, which coincides with the time when the hamburger was flipped. The peak mass concentration in Fig. 59, around 1 mg/m^3, is lower than the other meat scenarios, broiling hamburgers and frying bacon. The mass mean diameter is relatively constant, just below 0.2 μm, which is smaller than maximum mass mean diameter generated by broiling hamburgers and frying bacon, and closer to that of dark toast. Figure 60 shows the number concentration and the diameter concentration through the same frying hamburger test. The number concentration and the diameter concentration show similar trends to the mass concentration in Fig. 59. This particular test only had two alarm activations, both from new alarm models, but legacy alarms were activated in other frying hamburger tests.

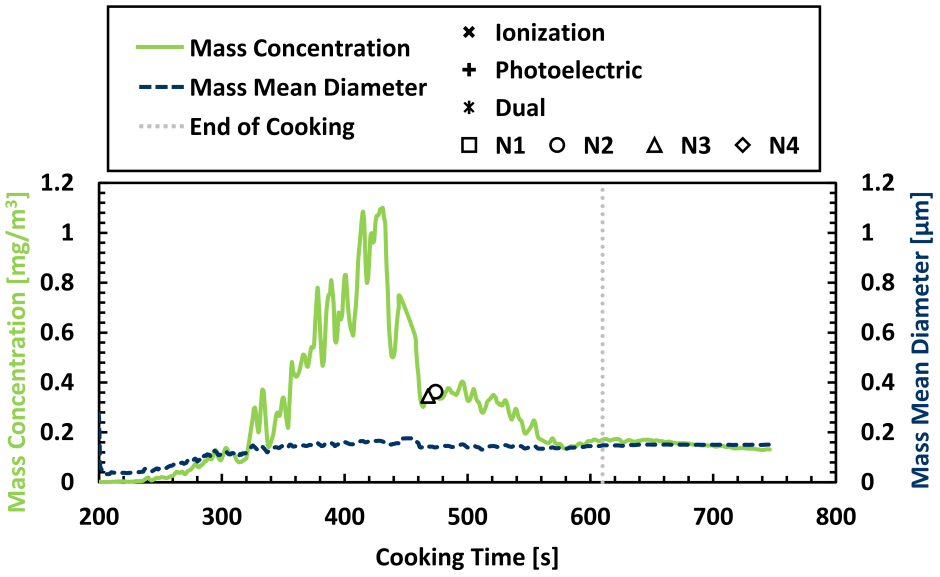

Fig. 59. The mass concentration and the mass mean diameter over the cooking time of one of the frying hamburger scenarios. Symbols indicate when alarm activated and the mass concentration at activation.

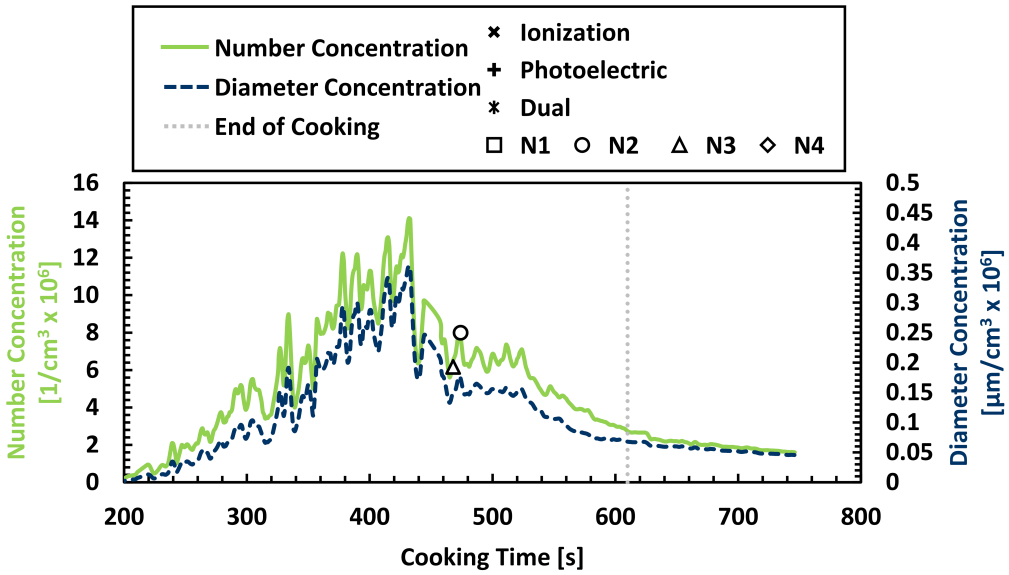

Fig. 60. The number concentration and the diameter concentration over the cooking time of one of the frying hamburger scenarios. Symbols indicate when alarm activated and the number concentration at activation.

Figure 61 shows the mass concentration and Fig. 62 shows the obscuration at alarm for the new alarms or the maximum values during the test if the alarm did not activate. The

average frying hamburger mass concentration at alarm for new alarms was 0.8 mg/m^3 with the range hood off. With the range hood on there were fewer activations (only model N2 during two tests), since the maximum mass concentrations were slightly lower than with the hood off. The average obcuration measured at alarm for the new alarms was 0.5 %/ft, which is at least half of the average obscuration at alarm for broiling hamburgers and frying bacon.

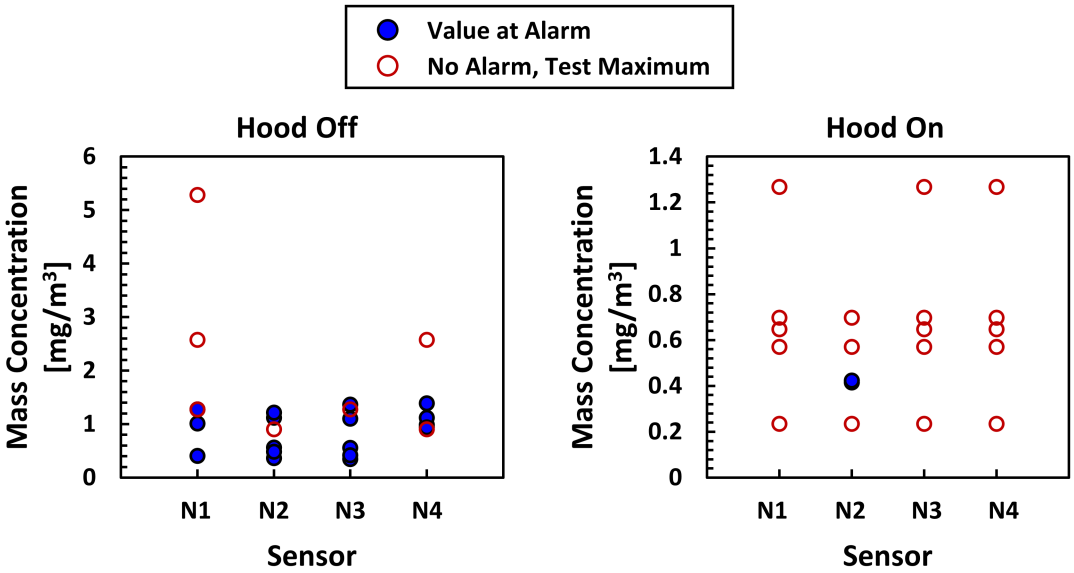

Fig. 61. Mass concentration at time of alarm (closed symbols) or at maximum mass concentration if no alarm (open symbols) for the N1, N2, N3, and N4 alarms with the hood off (left) and the hood on (right) for all frying hamburger tests.

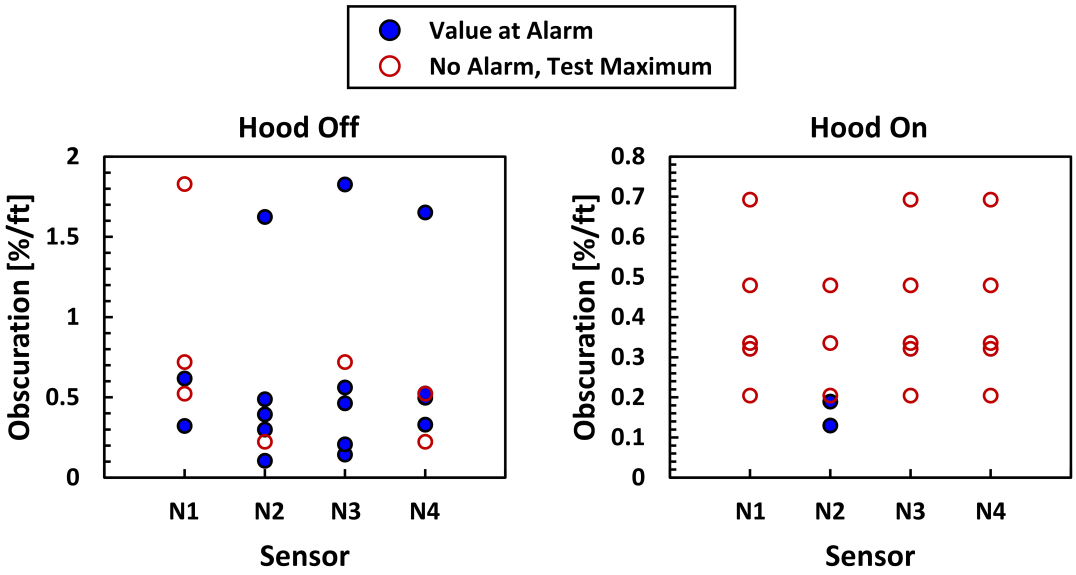

Fig. 62. Beam obscuration at time of alarm (closed symbols) or at maximum obscuration if no alarm (open symbols) for the N1, N2, N3, and N4 alarms with the hood off (left) and the hood on (right) for all frying hamburger tests.

The stir-fried vegetables cooking scenario had very low mass concentrations during most of the cooking time before increasing to moderate levels around the time the burner was shut off, as shown in the example mass concentration and mass mean diameter plot in Fig. 63. This particular test only produced one alarm after the end of the cooking time. The mass mean diameter also shows a significant increase between 700 s and 850 s in Fig. 63. Figure 64 shows the number concentration and the diameter concentration throughout the same stir-fried vegetables test. In contrast with the mass concentration, the number concentration varies less, increasing slowly from around 3 x 10^6 /cm^3 to 6 x 10^6 /cm^3 by the end of the test because of the simultaneous increase in the mass mean diameter of the particles. Figure 65 shows the mass concentration at alarm for the new alarms or the maximum concentration during the test if the alarm did not activate. The stir-fried vegetables tests had only one activation among all smoke alarms, with the hood off, for model N4. From Fig. 65, it can be seen that the mass concentration for the single activation, 2.4 mg/m^3 for model N4, was a higher value than all the other stir-fried vegetable tests.

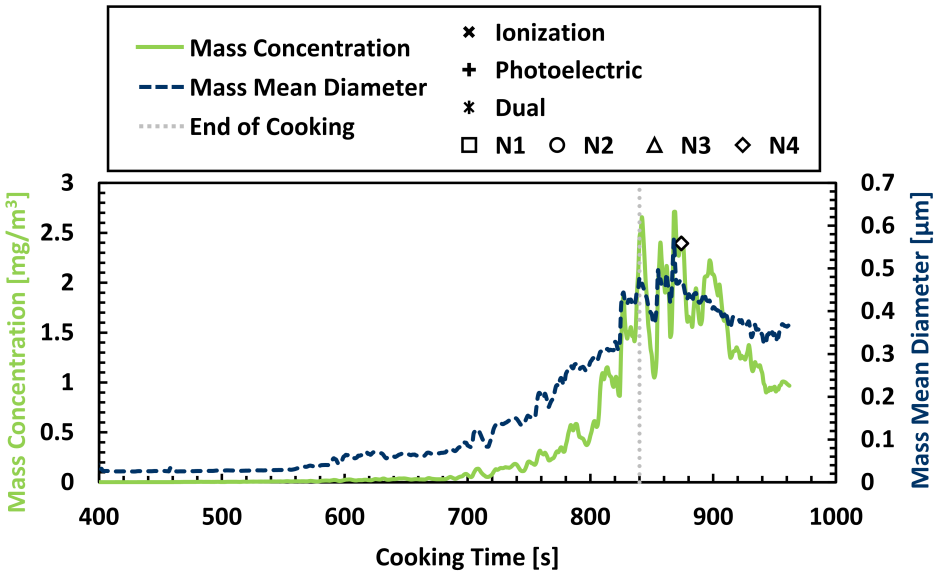

Fig. 63. The mass concentration and the mass mean diameter over the cooking time of one of the stir-fried vegetables scenarios. Symbols indicate when alarm activated and the mass concentration at activation.

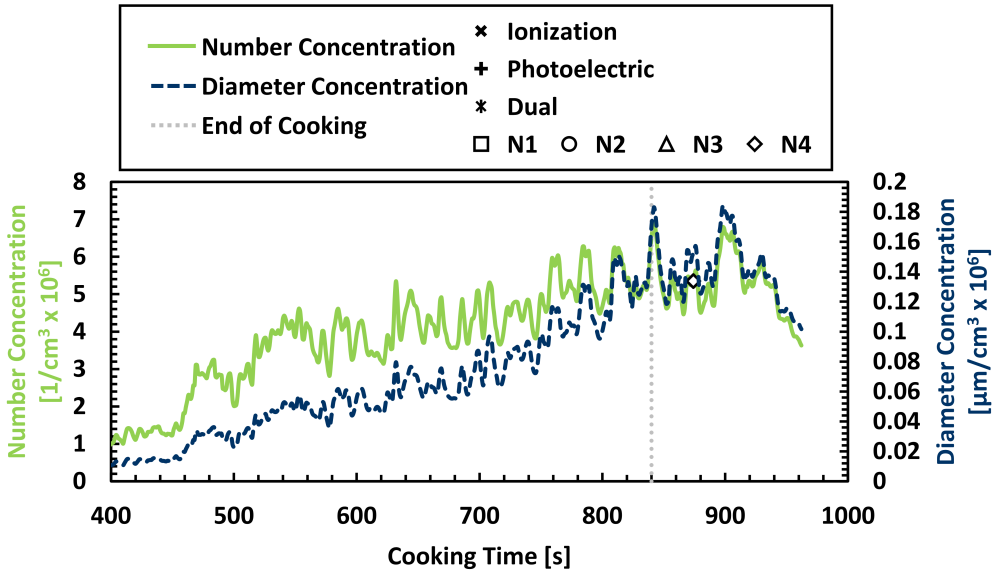

Fig. 64. The number concentration and the diameter concentration over the cooking time of one of the stir-fried vegetables scenarios. Symbols indicate when alarm activated and the number concentration at activation.

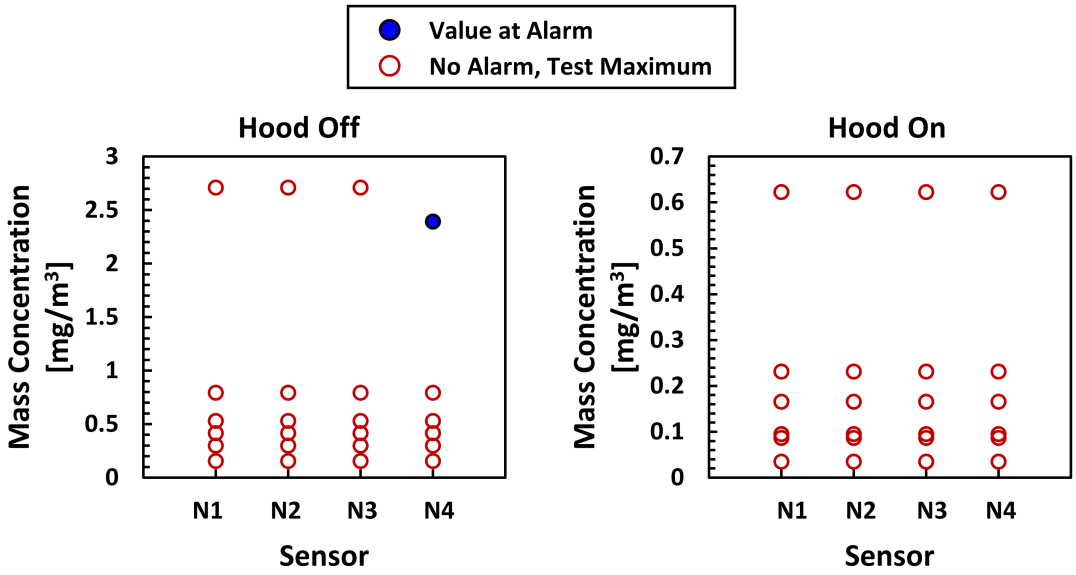

Fig. 65. Mass concentration at time of alarm (closed symbols) or at maximum mass concentration if no alarm (open symbols) for the N1, N2, N3, and N4 alarms with the hood off (left) and the hood on (right) for all stir-fried vegetables tests.

The mass concentration for the frozen potato fries test in Fig. 66 appears similar to the stir-fried vegetables, with low concentrations for most of the cooking time and a significant increase toward the end of cooking. One alarm activation, from model N4, was recorded close to the end of cooking time during the test in Fig. 66. The mass mean diameter, also in Fig. 66 is around 0.3 μm at 200 s when the mass concentration is very low, decreases to 0.05 μm at 400 s, and then slowly increases again to around 0.3 μm toward the end of cooking. The larger mass mean diameter towards the beginning may be a result of adding the frozen potato fries after preheating the oil for 120 s. Figure 67 shows the number concentration and the diameter concentration throughout the same frozen potato fries test. The mass concentration at alarm or the maximum concentration during the test is plotted in Fig. 68 for the new alarms. Again, model N4 was activated a few times during the frozen potato fries test when the hood was off and on, with the mass concentration at those times measuring around 1 mg/m^3 to 1.5 mg/m^3.

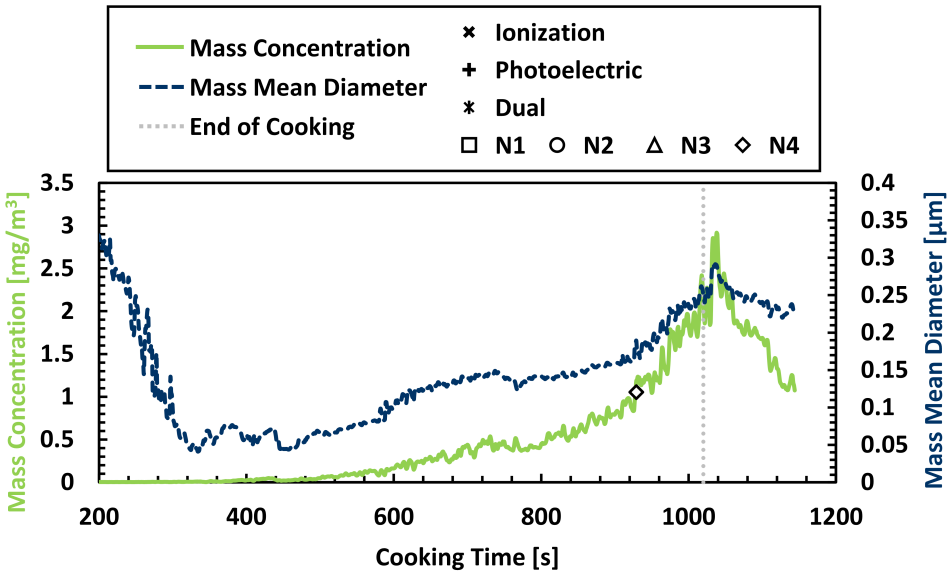

Fig. 66. The mass concentration and the mass mean diameter over the cooking time of one of the frozen potato fries tests. Symbols indicate when alarm activated and the mass concentration at activation.

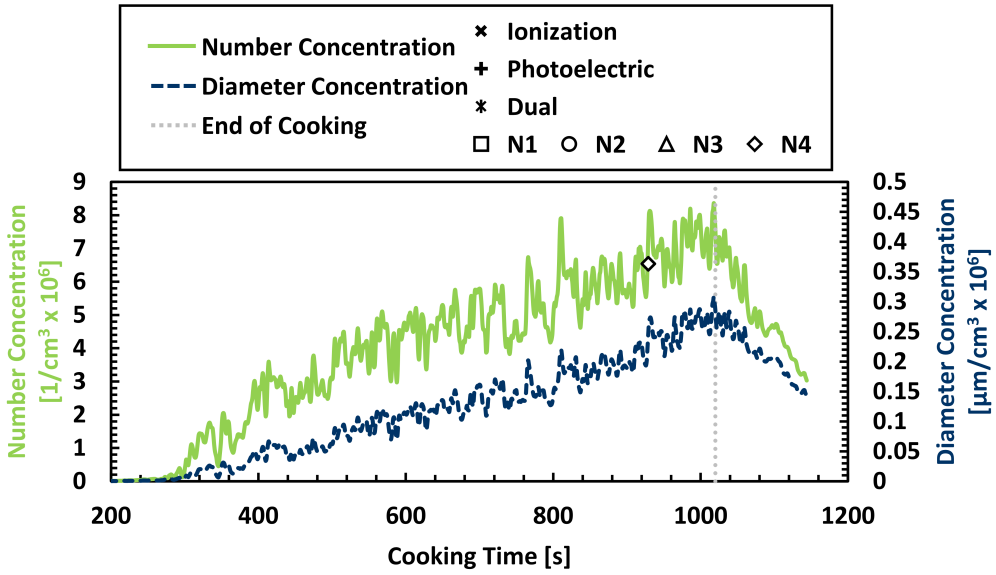

Fig. 67. The number concentration and the diameter concentration over the cooking time of one of the frozen potato fries tests. Symbols indicate when alarm activated and the number concentration at activation.

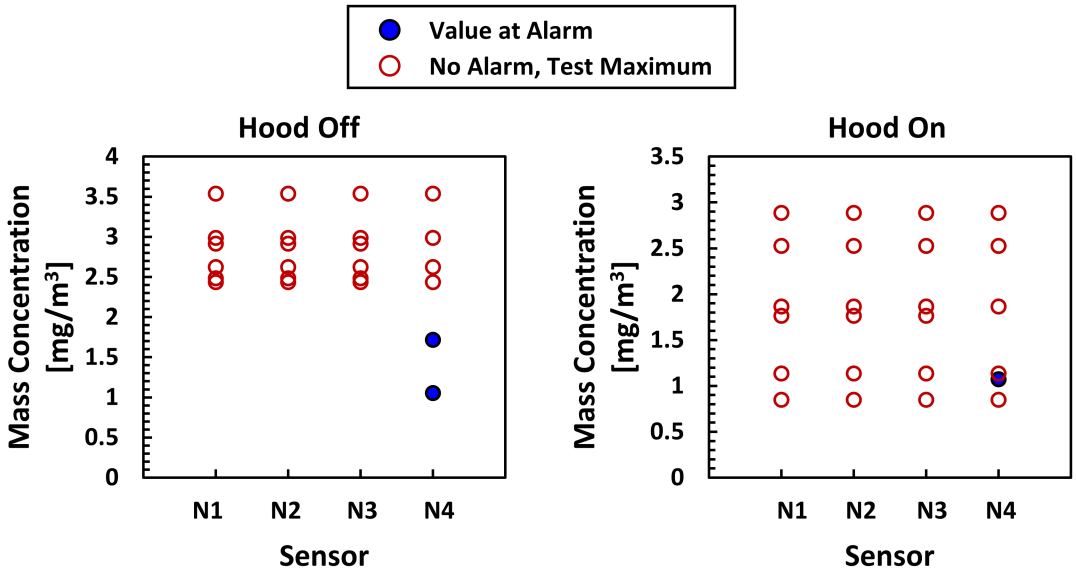

Fig. 68. Mass concentration at time of alarm (closed symbols) or at maximum mass concentration if no alarm (open symbols) for the N1, N2, N3, and N4 alarms with the hood off (left) and the hood on (right) for all frozen potato fries tests.

The mass concentration and mass mean diameter for the last cooking scenario, grilled cheese, is shown in Fig. 69 for a typical grilled cheese test. The grilled cheese scenario generated low aerosol mass concentration, with the peak values around 1 mg/m^3 occurring about 60 s after the end of cooking. The mass mean diameter measurement showed some variation, but remained below 0.25 μm. Figure 70 shows the number concentration and the diameter concentration throughout the same grilled cheese test. Since the mass mean diameter was relatively constant, the number concentration and diameter concentration show a gradual increase, similar to the mass concentration. None of the grilled cheese tests, including this test, produced any alarms for any smoke alarm models besides the closer reference alarms. Because there were no alarms during grilled cheese tests, Fig. 71 shows only the maximum mass concentration during each test because no alarms were activated in any grilled cheese tests. Besides one hood on test that had a maximum mass concentration of 2.8 mg/m^3, all grilled cheese tests had mass concentrations below 1.2 mg/m^3.

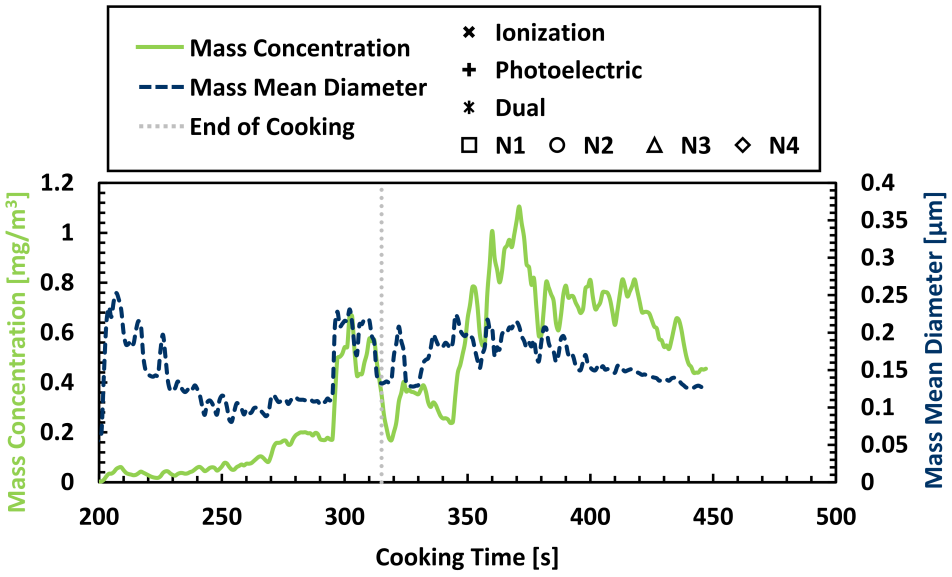

Fig. 69. The mass concentration and the mass mean diameter over the cooking time of one of the grilled cheese scenarios. Symbols indicate when alarm activated and the mass concentration at activation.

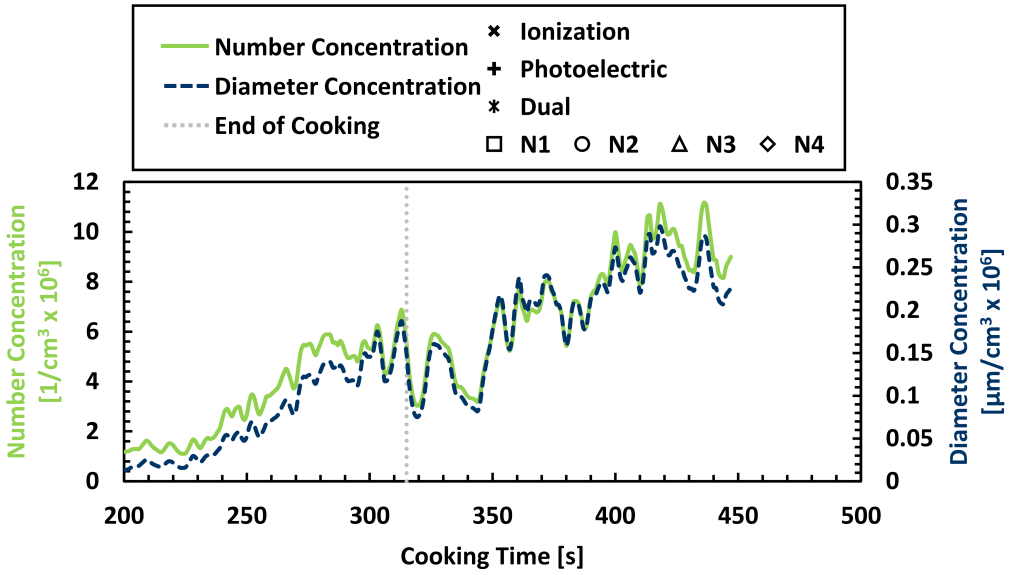

Fig. 70. The number concentration and the diameter concentration over the cooking time of one of the grilled cheese scenarios. Symbols indicate when alarm activated and the number concentration at activation.

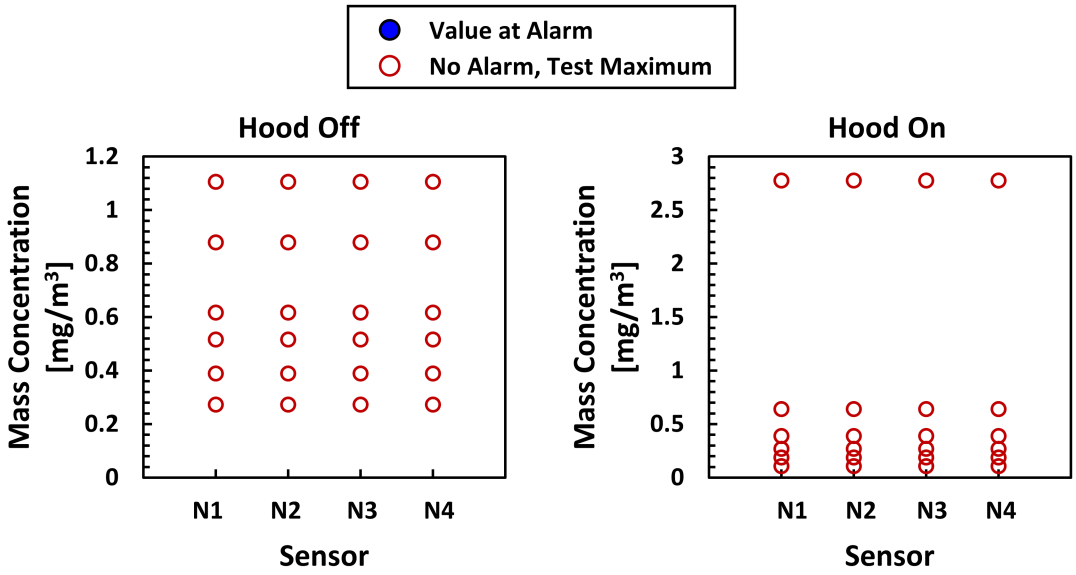

Fig. 71. Mass concentration at time of alarm (closed symbols) or at maximum mass concentration if no alarm (open symbols) for the N1, N2, N3, and N4 alarms with the hood off (left) and the hood on (right) for all grilled cheese tests.

4. Conclusion

This study exposed new and legacy smoke alarms of different types to a variety of selected cooking scenarios in a mock kitchen. The smoke alarm activation times were recorded, and the results were used to compare the nuisance resistance of new alarms to legacy alarms across a wider range of cooking sources than just the broiling hamburger nuisance test that was added to ANSI/UL 217. The fraction of tests that activated each smoke alarm was tabulated for tests with the range hood off and the range hood on.

While the mock-up kitchen was relatively small, the legacy dual (D2) alarm models that were closer to the cooking sources (the reference alarms) activated much more frequently than the other D2 alarm models. This observation, along with the overall reduction in propensity to alarm when the range hood was turned on, both reinforce the recommendation to maximize the distance from the nuisance source while still providing adequate coverage for smoke detection. While a legacy photoelectric-type (P2) was the alarm model which demonstrated the best overall resistance to the range of cooking aerosols with the range hood off, one of the new alarms (N3), along with another legacy photoelectric type (P1) and legacy dual type (D1), also performed well. All alarms showed marked improvement in performance when the range hood was turned on. Two of the new alarms that presumably relied either ionization chamber (N1) or light-scattering sensor (N3) designs, performed better than all other alarms when the range hood was on.

When grouping the alarm activation data by alarm type, it was observed that the new alarm group tended to behave similarly to the legacy ionization and photoelectric alarms with the hood on, and only slightly better than the legacy ionization alarms with the hood off. However, the legacy photoelectric alarm group performed the best overall across all tests. Given that the new alarms also need to meet the more stringent flaming and smoldering fire tests, it does appear that the cooking nuisance test provides a baseline performance level such that newer alarms do not perform worse than legacy alarms.

Aerosol concentration and size measurements also provided insight on the particle characteristics of the smokes generated by a broad range of nuisance sources. The mass concentration measured at the time of alarm activation varied between scenarios from around 1 mg/m^3 or less for frozen pizza, the toasting scenarios, frying hamburger, and frozen potato fries, to around 3 mg/m^3 or higher for broiling hamburgers, frying bacon and stir-fried vegetables. The aerosol measurements of number, diameter and mass concentration as well as the values at smoke alarm activation could provide guidance on future improvements to the next generation of smoke alarms.

References

[1] (2020) Underwriter's Laboratory, Northbrook, IL. UL/ANSI, 217 Standard for Safety Smoke Alarms. Available at https://standardscatalog.ul.com/standards/en/standard_217_8.

[2] Cleary TG (2016) A study on the performance of current smoke alarms to the new fire and nuisance tests prescribed in ANSI/UL 217-2015 (National Institute of Standards and Technology, Gaithersburg, MD), NIST TN 1947. https://doi.org/10.6028/NIST.TN.1947. Available at http://nvlpubs.nist.gov/nistpubs/TechnicalNotes/NIST.TN.1947.pdf

[3] Cleary T (2017) Particle Size Distributions from Smokes and Cooking Aerosols Sampled from Room Fire Experiments.

[4] (2016) Underwriter's Laboratory, Northbrook, IL. UL 858, Standard for Household Electric Ranges. Available at https://standardscatalog.ul.com/standards/en/standard_858_16.

[5] Ltd D (2021) Dekati® ELPI®+ User Manual, Ver 1.6.

[6] Järvinen A, Aitomaa M, Rostedt A, Keskinen J, Yli-Ojanperä J (2014) Calibration of the new electrical low pressure impactor (ELPI+). *Journal of Aerosol Science* 69:150–159. https://doi.org/10.1016/j.jaerosci.2013.12.006. Available at https://linkinghub.elsevier.com/retrieve/pii/S0021850213002528

[7] Mulholland G, Liu B (1980) Response of smoke detectors to monodisperse aerosols. *Journal of Research of the National Bureau of Standards* 85(3):223. https://doi.org/10.6028/jres.085.014. Available at https://nvlpubs.nist.gov/nistpubs/jres/85/jresv85n3p223_A1b.pdf